Study of crystal formation under solid-state aging conditions by high resolution electron microscopy

A thesis submitted to McGill University

in partial fulfilment of the requirements of the

degree of Master's in Chemistry

by

Anaïs Rose Hamelin

Department of Chemistry

McGill University

Montréal, Québec, Canada

December 2024

Table of content

Abstract

Mechanochemistry, a solid-state synthesis method, offers several advantages over solvothermal techniques, including shorter reaction times, higher selectivity, and reduced chemical waste. However, despite these benefits, its industrial-scale use for many crystalline materials has been limited due to an incomplete understanding of crystal growth processes. Gold nanoparticles (AuNPs), traditionally synthesized via solvothermal methods, are well understood in terms of their formation conditions, growth mechanisms, and kinetics. Their unique properties—optical activity, electrical conductivity, low toxicity, and high surface-to-volume ratio—make them highly useful for applications such as catalysis. Similarly, metal-organic frameworks (MOFs) are porous materials known for their applications in gas adsorption, storage, catalysis, and structural flexibility. The comprehension of the crystallinity of both NPs and MOFs is lacking when they are synthesized using a solid-state method. This thesis begins by reviewing the literature on mechanochemistry, focusing on the solid-state synthesis of nanoparticles and MOFs, along with issues related to crystallinity defects. It then investigates the characteristics of materials grown using solid-state methods. Specifically, the study examines the solid-state reduction and crystallization behaviors of AuNPs over a 15-day period, where the reactions are initiated with a small amount of mechanical energy in a controlled static environment. The effects of amine chain length and aging temperature on AuNP crystallinity and particle size are analyzed. To further explore the early-stage crystallization of solid-state-grown MOFs, techniques such as transmission electron microscopy (TEM), Powder X-Ray diffraction (PXRD) and energy electron loss spectroscopy (EELS) are used.

Résumé

La mécanochimie, une méthode de synthèse en phase solide, offre des avantages par rapport à certaines techniques solvothermiques; des temps de réaction plus courts, une sélectivité accrue et une réduction des déchets chimiques. Cependant, malgré ces avantages, son utilisation à l'échelle industrielle pour de nombreux matériaux cristallins reste limitée en raison d'une compréhension incomplète des processus de croissance cristalline. Les nanoparticules d'or (AuNPs), traditionnellement synthétisées par des méthodes solvothermales, sont bien documenté en ce qui concerne leurs conditions de formation, leurs mécanismes de croissance et leur cinétique. Leurs propriétés uniques, telles que l'activité optique, la conductivité électrique, la faible toxicité et un rapport surface/volume élevé, les rendent très utiles pour des applications comme la catalyse. De même, les cadres organométalliques (MOFs) sont des matériaux poreux connus pour leurs applications dans l'adsorption de gaz, le stockage, la catalyse et leur flexibilité structurelle. Cependant, la compréhension de la cristallinité des NPs et des MOFs est insuffisante lorsqu'ils sont synthétisés par des méthodes en phase solide. Cette thèse commence par une revue de la littérature sur la mécanochimie, en se concentrant sur la synthèse en phase solide des nanoparticules et des MOFs, ainsi que sur les problèmes liés aux défauts de cristallinité. Elle explore ensuite les caractéristiques des matériaux produits par des méthodes en phase solide. Plus précisément, l'étude examine la grosseur et cristallisation des AuNPs en phase solide sur une période de 15 jours, où la réaction est initiées par une petite quantité d'énergie mécanique dans un environnement statique contrôlé. Les effets de la longueur des chaînes d'amines et de la température de vieillissement sur la cristallinité et la taille des AuNPs sont analysés. Pour explorer plus en détail les premiers stades de la cristallisation des MOFs produits en phase solide, des

techniques telles que la microscopie électronique à transmission (TEM), diffraction des rayons X de la poudre (PXRD) et la spectroscopie de pertes d'énergie d'électrons (EELS) sont utilisées.

Acknowledgement

I thank the Natural Science and Engineering Research Council of Canada (NSERC) - Discovery Grant and Discovery Accelerator Supplement, the Canada Foundation for Innovation (CFI), the Fonds de Recherche du Québec - Nature et technology - Centre for Green Chemistry and Catalysis (CGCC), and McGill University for their financial support.

I would like to thank some technical facilities throughout McGill for their training and access to analytical devices. Thank you to the Facility for Electron Microscopy Research (FEMR) of McGill University, to the MC^2 facility at McGill University, to the McGill Institute for Advanced Materials (MIAM). There are people who work at these facilities that I would like to thank as well. Thank you to Dr. Hatem Titi from MC2 for your training and assistance with powder X-ray diffraction (PXRD) as well as all the scientific input you were able to provide. Thank you to Dr. Jesus Valdez from FEMR for your training and assistance with scanning transmission electron microscopy (STEM), transmission electron microscopy (TEM) and Electron energy loss (EELS).

Thank you to all members of the Moores research group that I have met. Most specifically thank you to the members I interacted with the most. Thank you Galen for indulging me in many debates and conversations. Thank you to Sara for always being an amazing friend always available for appreciated emotional support. Thank you, Austin, for making my days more interesting with your lovely personality and useful insights. Thank you, Jasmine, for always finding ways to make me laugh and for having such a calming personality. Thank you Ruby for your kind smile and crafty spirit. Thank you Justine for your awesome desserts and great encouragements. Thank you Ishneet for the ray of sunshine you bring to our group. Thank you Maddison, Lila and Maddy for being awesome friends outside of my own group, always there to give tips and tricks that only an outside point of view can provide. Thank you to all visiting students, Daniella, Renzo, Kiran and Pravin

for expanding my knowledge and allowing me to introduce all of you to the Quebec culture. Thank you Freyja for giving me pawsitive energy throughout the last year and a half. I could always count on you to make my days interesting. Thank you Christopher for being my first friend in this new town. Thank you Ben for your support during the last year. I can only hope I will be able to give you the same kindness and patience when you are writing your own thesis.

To my best friends Eve and Chris (Steve); I wanted to take a moment to express how truly grateful I am to have you in my life. Thank you for always being there for me—through the ups and downs, the laughter and tears, the lively nights and gloomy mornings, and through every wins and loses. Your unwavering support means the world to me, and I honestly don't know what I would do without you guys. Every adventure we've shared has made my life so much richer. I appreciate your kindness, your understanding, and the way you always know how to make me smile. Thank you for accepting me as I am and for inspiring me to be my best self. I cherish every memory we've created together and look forward to making many more.

To Mom and Dad, all of your love, support, and encouragement during these past 6 years have meant the world to me. Every step of the way, through facetime dinners and emotional rants, you've been there, and it has made all the difference. Mom and Dad, you've always believed in me, even when I doubted myself. Your sacrifices, your wisdom, and your unwavering faith in me have been my greatest motivation. You've given me the courage to chase my dreams, knowing that no matter what, I have you to lean on. To every family member, I hope you know how much I love you all. I truly couldn't have made it this far without you, and I'm so blessed to have you as my family.

Finally, I have to thank myself for my patience and perseverance.

I promise to be gentler with myself in the future.

Contribution of authors

Austin Richard helped with experimental design and editing the manuscript

Sammohith Nittala and Prof. Nikolas Provatas helped with experimental design and discussion on mechanistic aspects.

Dr. Jesus Valdez helped with the collection of TEM data for this work.

Prof. Audrey Moores helped with experimental design, supervision and editing the manuscript.

All authors played a role in the editing of the manuscript prepared by me.

Chapter 3

Austin J. Richard helped with experimental design and editing the manuscript.

Hudson Bicalho helped with experimental design and editing the manuscript.

Prof. Ashlee Howarth helped with experimental design.

Prof. Audrey Moores helped with experimental design, supervision and editing the manuscript.

List of figures

List of tables

1 Introduction

This chapter serves to prepare and inform the reader for Chapters 2 and 3, which present the manuscript-based portions of this thesis. It provides essential scientific background and context, drawing upon a comprehensive review of relevant literature. Key discussed concepts include aging, mechanochemistry, nanoparticles, metal-organic frameworks (MOFs), crystal defects, and high-resolution transmission electron microscopy (HR-TEM), all of which are critical for understanding the foundation of this research. To achieve a deeper understanding and an enhanced control over the solid-state mechanosynthesis, we endeavoured to study crystalline growth through these two primary objectives: (1) to explore the size and crystallinity behaviour of gold nanoparticles, and (2) to investigate the early-stage crystallisation of UiO-66, both objectives being explored within solid-state systems. The use of solventless imaging via HR-TEM enabled visual analysis of both systems, providing valuable insights into their structural properties.

1.1 Solid-state synthesis; Mechanochemistry and Aging

Mechanochemical reactions are reactions that are initiated or driven by mechanical energy.[1] The use of mechanochemistry allows for a reaction that doesn't require bulk solvent, which often have an impact on the environment and the reaction itself.[2] Materials synthesized in the solid-state often feature enhanced selectivity, high atom economy, and improved energy efficiency.[3] To utilize these advantages to their maximum potential, it is important to understand how mechanochemical and aging-based transformations behave differently from more traditional solvothermal chemistry. Numerous instruments can be used in a mechanochemical reaction such as the mortar and pestle,

vibrational mill and twin-screw extruder[4] (Fig. 1.1).[1, 5] Metal-organic frameworks,[6,7,8] nanoparticles,[9] photocatalyst,[10] quantum dots[11,12] and co-crystals[13] are some examples of materials that can be made using mechanochemistry. All these materials have their properties highly regulated by their crystallinity, making them good candidates for studying crystalline growth in the solid state.

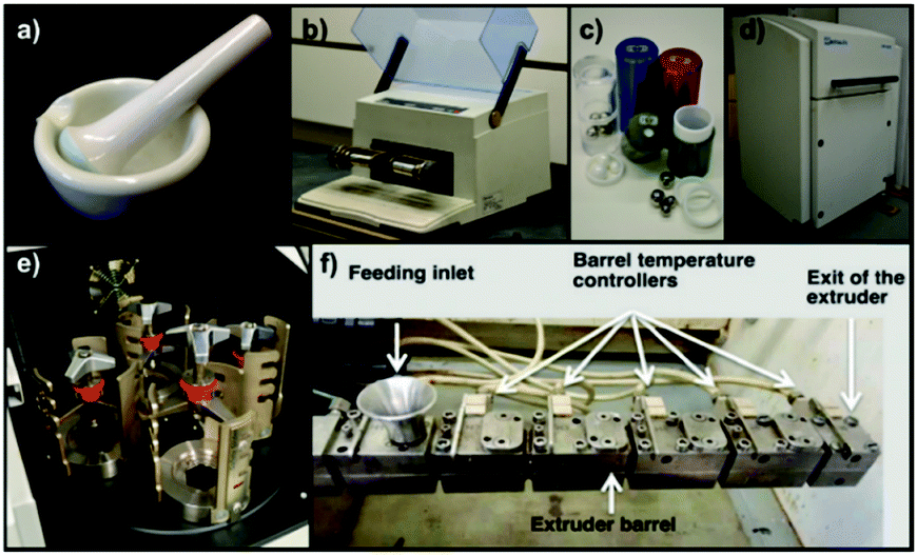

Figure 1.1 Equipment for mechanochemical reactions (a) mortar and pestle (b) vibrational mill and (c) small-scale milling jars and balls (d) planetary mill external and (e) internal (f) twin-screw extruder (TSE) allowing for continuous processing. 1a, 1b, 1c, 1d and 1e used with permission of Royal Society of Chemistry, from Ref. 5; permission conveyed through Copyright Clearance Center, Inc. 1f used and adapted from Ref. 4 with permission from the Royal Society of Chemistry.

Mortar and pestle is a well-known instrument for mechanochemistry with its first usage going back to the prehistoric age. Mortar and pestle is an inexpensive synthesis method which has drawbacks, such as lack of consistency and low yield. In 1960, Dachille and Roy converted calcite to aragonite by long exposure to mortar and pestle grinding.[14] Treece et al. used a mortar and pestle and temperature ignition to synthesise GaP and GaAs in a solid-state system.[15] Grinding the gallium iodide and sodium pnictide precursors individually before combining them ensures a more evenly distributed force during the grinding process. After igniting the powder combining both precursors, the mixture was ground manually by mortar and pestle in a drybox, resulting in GaP or GaAs

depending on the pnictide used as a precursor.[15] The use of mortar and pestle in some reactions also allowed for the accessibility of compounds which were inaccessible by a solution synthesis. Patil et al. T demonstrated that a mortar and pestle provided enough mobility and energy in the synthesis of quinhydrones to form a new product without producing its more stable isomer.[16]

This was one of the first demonstrations of the possibility of better selectivity when using solid-state chemistry compared to solution synthesis.[16] The mortar and pestle has since been replaced by a mortar grinder, which allows for better reproducibility and the introduction of temperature variations.[17]

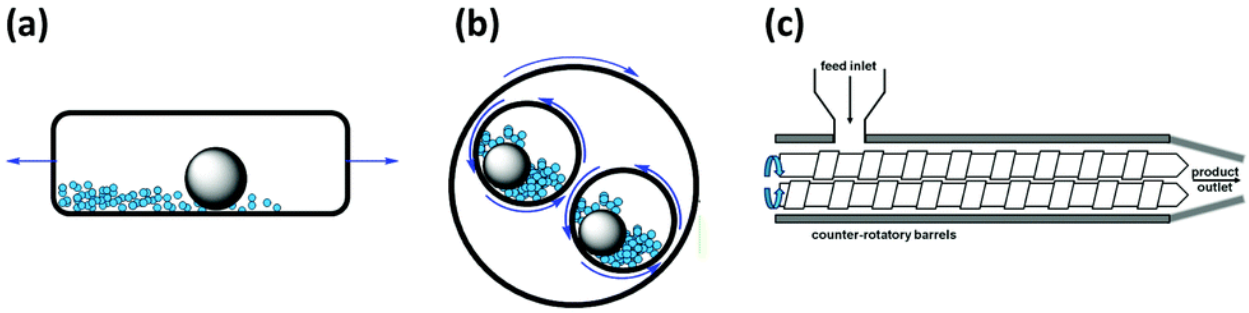

Figure 1.2 Schematic representation illustrating the mode of motion of the cross-section of a (a) shaker and (b) planetary mill, and (c) twin-screw extruder. Reproduced from Ref. 1 with permission from the Royal Society of Chemistry.

Another common instrument used in mechanochemistry is the ball mill, which uses ball bearings of different sizes and materials as grinding media to impact mechanical force on the reagents (Fig. 1.2). The shaker mill is used for small scale reactions and grinds by impacts and friction. Its large-scale counterpart, the planetary mill, uses centrifugal force to high energy grinding also by impact and friction.[17] There is also the cryo-mill, which is a mixer mill cooled thanks to free-flowing liquid nitrogen flown around the jar to allow both cryogenic grinding and trapping volatile compounds during milling.[17]

Aging may complement mechanochemical synthesis. Aging involves the use of specific reaction conditions in which the reaction is driven thermally in the solid state, sometimes complemented with different conditions such as humidity, solvent vapour, movement, light and pressure.[18] Vapor assisted aging is a technique that uses solvent vapour or humidity to age a sample. Usually, a beaker full of volatile solvent is placed in an air-tight container with the sample. This allows for the powder to have more mobility, which accelerates or initiates the reaction.

Štrukil developped a hydrolysis of waste polyethylene terephthalate PET treatment either by mechanochemistry or by aging.[19] Starting by milling with pre-milled PET and sodium hydroxide in a jar with a steel milling ball for 60 minutes, a Fourier-transform infrared attenuated total reflection (FTIR-ATR) showed evidence of terephthalic acid (TPA) disodium salt. After workup, PET conversion was high as was TPA yield even without the usual harsh conditions needed.[19] They then tested the same reaction but with vapor-assisted aging (Fig. 1.3).

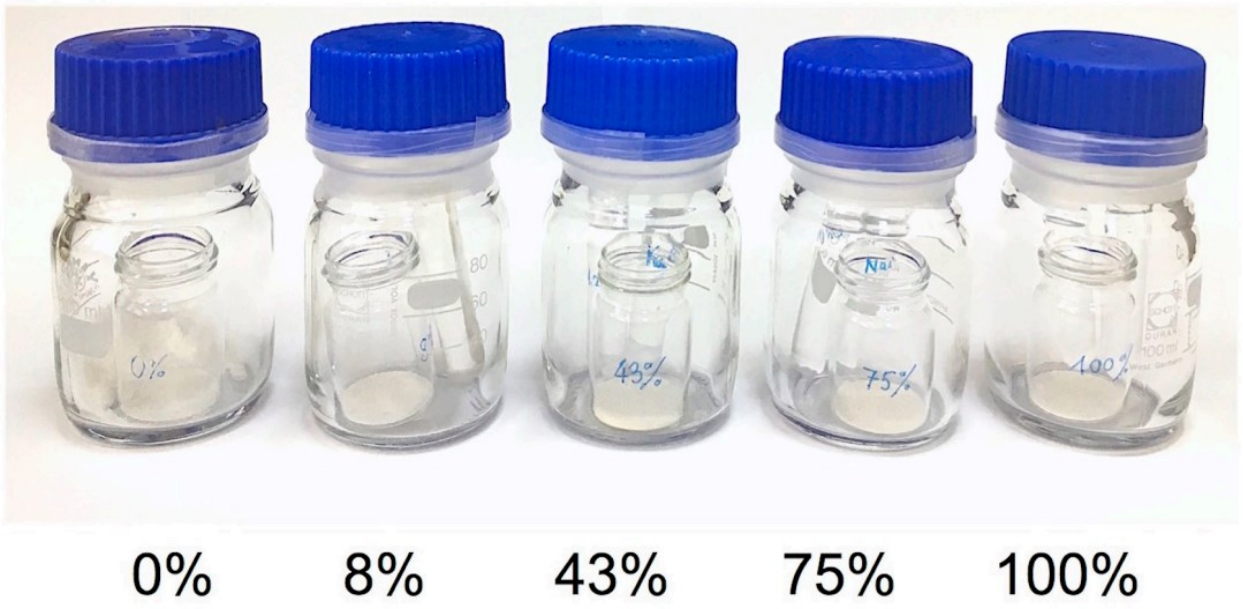

Figure 1.3 Reaction setup for the solid-state alkaline PET hydrolysis by aging at different levels of relative humidity (100 mg PET scale). Aqueous salt solutions were put in two small test tubes inside the aging chambers. For aging in organic vapours, the test tubes inside the aging chambers. For aging in organic vapours, the test tubes were filled with dry acetonitrile, 1,4-

dioxane, methanol or ethanol. Reprinted from Ref. 19, permission provided by John Wiley and Sons and Copyright Clearance Center

They found that under aging conditions with high relative humidity (RH) for an extended period, the conversion rate was higher than at lower RH or with a significant decrease in aging time. Heating the mixture to 100°C or premixing the reagents for 5 minutes was shown to enhance PET depolymerization under aging conditions.[19]

Another alternative to add mobility to a mechanosynthesis is the addition of solvent to the system during milling.

1.2 Milling Additives: Solid solvent, LAG and ILAG

In a ball mill, the addition of the milling balls can have a great influence on the results of the reaction. Balls of different sizes can affect the surface contact of the ball to the sample and so change the outcome of the milling. Michalchuk et al. found that a ball of bigger size and mass resulted in a faster transformation in the jar during a mechanochemical synthesis.[20] The group associated that with a larger amount of powder being influenced by the greater contact with the ball.[20] They also determined that a reaction would also go faster if the mass of the milling ball was higher.[20] Fischer et al. also concluded that a heavier and bigger ball moderately increased the temperature of the system after a long milling time.[21] To control the thermal equilibrium inside the jar, one might be tempted to choose a smaller, lighter milling ball, freeze the jar before milling or even shorten milling time.[22]

Some mechanochemical reactions use a technique called liquid-assisted grinding (LAG). This refers to the addition of a catalytic amount of liquid added to the sample before grinding, inducing reactivity to an otherwise unreactive system. Whether the addition of solvent to a mechanochemical reaction is classified as a LAG reaction depends on the ratio of microliters of

solvents to milligrams of solid (η). The η ratio for LAG is between 0-2 µL/mg while a reaction in solution would have a η value of more than 12 µL/mg (Fig. 1.4).[5] It is also important to note that a η value of 0 is considered a neat reaction because it is done with the complete absence of solvent.[23]

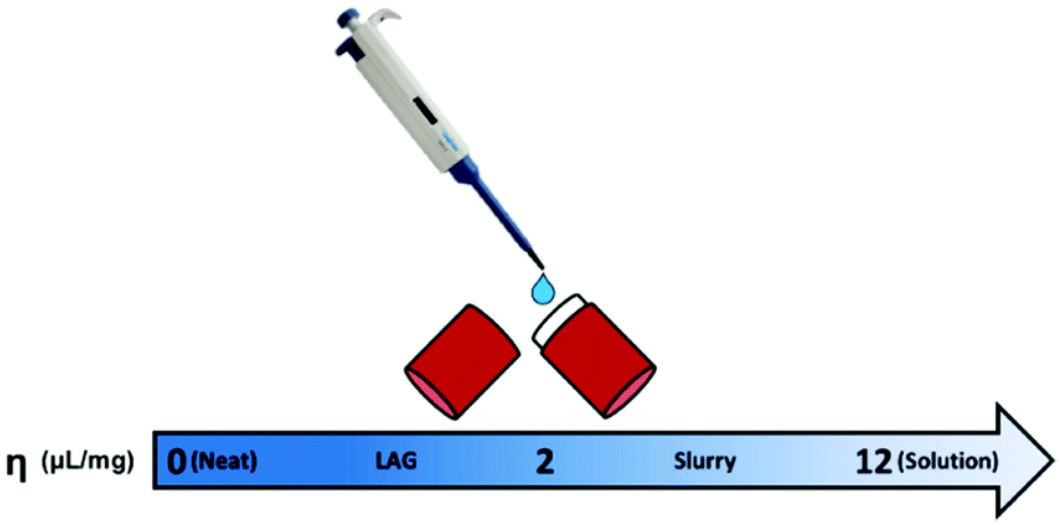

Figure 1.4 Schematic showing the range of η values, from neat grinding at 0 µL mg^{-1} to ≥12 µL mg^{-1} for solution chemistry. Used with permission of Royal Society of Chemistry, from Ref.13; permission conveyed through Copyright Clearance Center, Inc.

Chen et al. used LAG to gain access to a much greater selectivity in the palladium-catalysed dimerisation of terminal alkyles.[24] The use of a palladium catalyst in the reaction was found to be an alternative to the use of a copper catalyst because of the significantly smaller amount of palladium needed to make the reaction go forward. Unfortunately, this replacement also greatly reduces the selectivity of the reaction, with the desired 1,3-diyne dimer usually accompanied by three more enyne byproducts.[24] Using LAG, the reaction conditions showed the possibility of switching the selectivity from the diyne into the trans-enyne.[24]

Another popular method is ion and liquid assisted grinding (ILAG). These methods use a catalytic amount of salt additive, around 5 mol%, for the milling process. The inclusion of ionic additives

frequently increases the range of topologies that can be achieved through mechanochemical synthesis. It is often used for synthesis of zeolitic imidazolate frameworks (ZIF), a group of zinc based metal-organic framework.[25] This MOF is ideal for ILAG synthesis because the selection of additives can change the structure of the MOF and dictate which ZIF is formed.

Friscić et al. used LAG and ILAG for the synthesis of well-known MOFs based on terephthalic acid.[25] They found that grinding the reagents together without LAG did not provide a crystalline MOF. After incorporating dimethylformamide DMF in catalytic quantities prior to milling for the same amount of time, the resulting MOF exhibited a different isomer from that produced during the solvothermal process. The addition of $NaNO_3$ to the reagents showed that ILAG formed a mix of two isomers, with the isomer usually observed by solvothermal reaction becoming more prominent with increasing milling time. The formation of the two MOF isomers was analysed and confirmed by PXRD, FTIR, solid state NMR. The group tested a multitude of other salts for the same reaction and found that the addition of salt to the system accelerated and directed the formation of MOFs.[25] Some salts, like NH_4NO_3 and K_2SO_4, gave the ILAG more selectivity.[25]

A more recent advancement is the use of a solid solvent in a mechanochemical reaction. A dry solvent, sometimes also called auxiliary, should not participate in the reaction but should allow for even mixing and deaggregation of a sample in the mill. A good indication of the need to use it would be the observation of a shell on the milling ball (Fig. 1.5).[26] Yang et al. used NaCl and KCl as a solid solvent in a one pot synthesis of HKUST-1.[26] They were able to make a pore and function adjustable HKUST-1 by combining 1,3,5-benzenetricarboxylic acid (H_3BTC) and copper acetate monohydrate with a solid solvent separately before pre-grinding. They then milled both pre-grind powders together for 20 minutes before washing the powder, resulting in high yield porous MOF.[26]

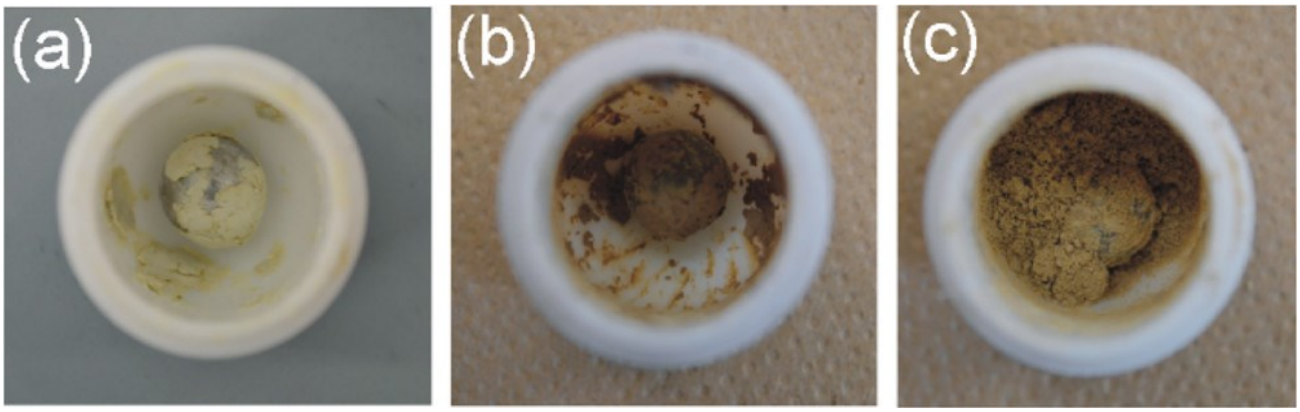

Figure 1.5 Reaction mixture (3a, 2 mol % D) after LAG with and without a solid auxiliary: aggregation on the milling ball (a) after 15 min, (b) after 5 h, and (c) after 2 h of milling with NaCl (34% yield). Reprinted with permission from Ref 28. Copyright 2015 American Chemical Society

Pentecost et al. also used NaCl in nanodiamond powder synthesis. The salt was used as a deaggregation agent, allowing for the avoidance of microbeads usage. Avoiding powder aggregation also allowed the particles to be separated by size, a big factor in the application of nanodiamond.[27] Do et al. developed a high-yielding ruthenium catalysed olefin metathesis.[28] While it was established that milling styrene, a liquid, resulted in a fast cross-metathesis, they wanted to test the milling of methyl 4-vinylbenzoate and 4-vinylbenzoic acid. During the LAG of both solids, the yield for methyl 4-vinylbenzoate was found to have considerably improved while the reaction of 4-vinylbenzoic acid gave subpar and irreproducible results. To improve the reactions further, they added 150% of the total reactant weight in solid solvent. They used a variety of grinding auxiliary with NaCl giving the best yield and NaBr giving the worst. [28] Sodium chloride has been a well-known choice for dry solvent because of its removal simplicity. Sugar is also known to be useful for the same purpose.

1.3 Bottom-up and Top-down Mechanical Synthesis of Nanomaterials

Nanomaterials (NMs) are defined as structures with at least one dimension within the nanometer range, typically between 1 and 100 nanometers. A variety of substances, including metals, semiconductors, polymers, and biological molecules, can be engineered at the nanoscale. The reduced size and increased surface area-to-volume ratio of NMs impart distinctive properties that are not observed in their bulk equivalents, making them exceptionally versatile and suitable for applications across numerous scientific and industrial fields. NMs can be synthesized using two primary mechanical synthetic approaches: Bottom-up and top-down syntheses (Fig. 1.6). The bottom-up method aims to make NMs out of a molecular precursor similar to solvothermal synthetic methods. This method is able to nucleate metal atoms which in turn produce observable nanoparticles. More milling time usually produces bigger particles in this regime, and as such a smaller surface-area-to-volume ratio. Bottom-up synthesis has been shown to shows good promise for the control of NMs definition, shape, composition and physiochemical features.[29]

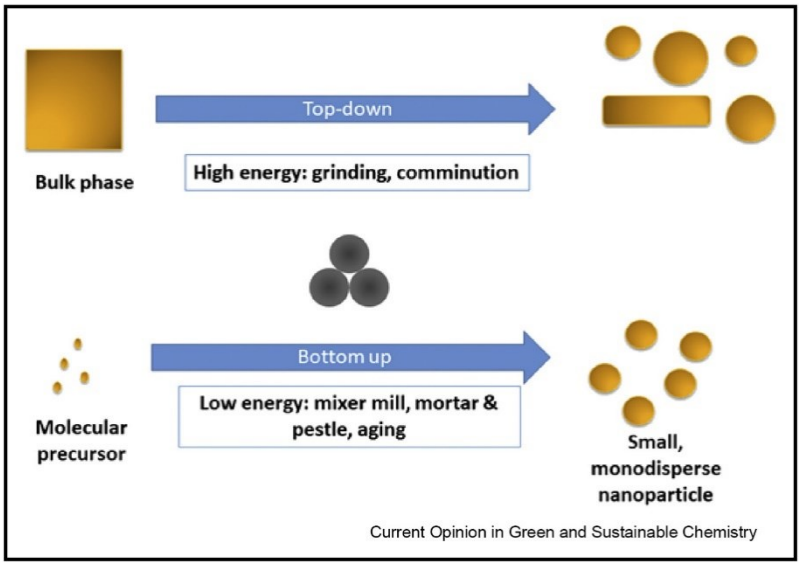

Figure 1.6 Top-down (top) and bottom-up (bottom) strategies in solid-state nanoparticle synthesis. Reprinted from Ref.30, Copyright 2018, with permission from Elsevier.

Bottom-up mechanochemical synthesis has been used by many to synthesize biological samples such as amino acids and materials such as NPs.[30] Lin et al. reported the solventless mechanochemical synthesis of silver NPs on carbon nanotubes.[31] Multiwalled carbon nanotubes (MWCNTs) and silver acetate were milled together in a zirconia jar and analyzed through scanning electron microscopy (SEM). The silver NPs were found to be homogeneously distributed on the nanotube surface. They found that their technique was also applicable to other carbon substrate and other metal salts.

The top-down approach involves milling and grinding the bulk materials to produce fine small particles. The bulk material is put in a device which provides mechanical stress to break the big structures down and induce plastic deformation with more time under stress. While this technique has drawbacks such as lack of size control and uneven surfaces, it has an important advantage; it is very simple. [32]

Lin et al. use the top-down method to prepare high-surface-area carbons (HSACs).[33] The need to find an alternative to the addition of harmful activating agents who also generate low yields and contaminated activated carbons (ACs), material commonly used to filter contaminants. Traditional methods using mechanical activation produce ACs with low surface-area, which limit their possible uses. To remedy this, shredding renewable resources such as coconut shells (CS) forms mechanochemical coconut shells (MCS), irregularly sized particles rich in oxygen-containing groups.[33] Adding the MCS to a 900 °C for 9 h carbonised the particles (HSAC-MCS-900-9) and generated small particle sizes analysed by SEM. After N_2 adsorption-desorption and density functional theory (DFT) analysis revealed that the HSAC-MCS-900-9 had a good amount of micropores at 1.3 nm with the occasional presence of meso- and macro- pores ranging from 2 to 127 nm. A Brunauer-Emmett-Teller (BET) surface area analysis revealed the out-performance of

HSAC-MCS-900-9 compared to other ACs because of its high surface area and large pore volume.[33]

1.4 Solid-state growth; Nanoparticles and Metal-Organic Frameworks

Nanoparticles (NPs) are a class of NMs with three-dimensions below 100 nm that are often used in catalytic capacities[34,35], biological settings[36,37], cancer treatment and detection[38], and more. Since NPs have such a variety of uses, researchers usually select their synthesis method based on the properties desired. Amongst the various methods, chemical reduction is widely used for synthesising metallic nanoparticles, such as gold, silver, and platinum nanoparticles.[39]

Debnath et al. developed the first gold nanoparticles (AuNPs) solid state synthesis in 2009.[40] Combining $KAuCl_4$, sodium borohydride and Poly(vinylpyrrolidone) in an agate container with an agate milling ball mixed at 1500 rpm for varying amounts of time resulted in a bottom-up synthesis of AuNPs. The sodium borohydride, acting as reducing agent, and Poly(vinylpyrrolidone) acting as protective ligands, reducing the agglomeration and controlling the size and shapes of the formed AuNPs.

Table 1.1 The experimental conditions for the synthesis of the gold nanoparticle samples and their corresponding sizes. Used with permission of Royal Society of Chemistry, Ref.40; permission conveyed through Copyright Clearance Center, Inc.

Sample	Mass ratio of $KAuCl_4$: PVP : $NaBH_4$	PVP [a]/kg mol^{-1}	Time/min	Particle diameter/nm
A	10 : 25 : 1	10	15	8.8 ± 2.8
B	10 : 25 : 1	10	30	10.7 ± 1.1
C	10 : 25 : 1	10	60	13.4 ± 2.4
D	10 : 25 : 1	10	120	23.3 ± 5.0

Sample	Mass ratio of $KAuCl_4$: PVP : $NaBH_4$	PVP [a]/kg mol^{-1}	Time/min	Particle diameter/nm
E	10 : 25 : 1	~30	15	6.3 ± 2.1
F	10 : 25 : 1	~30	30	7.5 ± 2.4
G	10 : 25 : 1	~30	60	8.4 ± 2.7
H	10 : 25 : 1	~30	120	8.8 ± 3.4
I	5 : 25 : 1	10	15	7.6 ± 2.3
J	5 : 25 : 1	10	30	8.3 ± 2.9
K	5 : 25 : 1	10	60	8.6 ± 2.3
L	5 : 25 : 1	10	120	11.8 ± 4.4
M	15 : 25 : 1	10	15	27.9 ± 6.2
N	15 : 25 : 1	10	30	N.A.[b]

a Mass average molar mass. b Aggregation of particles was observed.

Diffuse reflectance spectroscopy (DRS), transition electron microscopy (TEM) imaging and FTIR characterised the AuNPs formed while PXRD was used to confirm the growth of AuNPs in the solid system. The results showed that varying the reagents mass ratios, reaction time, and mass average molar mass of the protective ligand can alter the size of the particles. The group was able to form stable NPs with sizes ranging from 6.3 nm and 27.9 nm.[40] Richard et al. developed a solid-state synthesis of AuNPs through a modified Turkevich reaction.[22] Aging a grinded sample containing $HAuCl_4 \bullet 3H_2O$, octadecylamine (ODA) and trisodium citrate dihydrate, they found that the growth of AuNPs was stunted at -18 °C and accelerated at 32 °C.[22] Rak et al. reported a fast galvanic-reduction mechanochemical reaction able to produce gram amounts of AuNPs.[9] Using different lengths amine chains resulted in the synthesis of different sized monodispersed

AuNPs with the shorter chain amine resulting in bigger AuNPs. Their approach necessitated a significantly lower amount of solvent compared to conventional synthesis methods, resulting in the production of previously unattainable amine-stabilized ultra-small AuNPs.[9]

Metal-organic frameworks (MOFs) are porous structures combining metal clusters and organic linkers (Fig. 1.7).[41] The MOFs pores and high surface area are some of the characteristics of this hybrid material that makes them so interesting.[42] These materials have a flexible design that allows for a customisation of properties.[43] Because of this, there has been a good deal of new research focused entirely on developing MOFs for catalytic, gas storage and drug delivery purposes.[41]

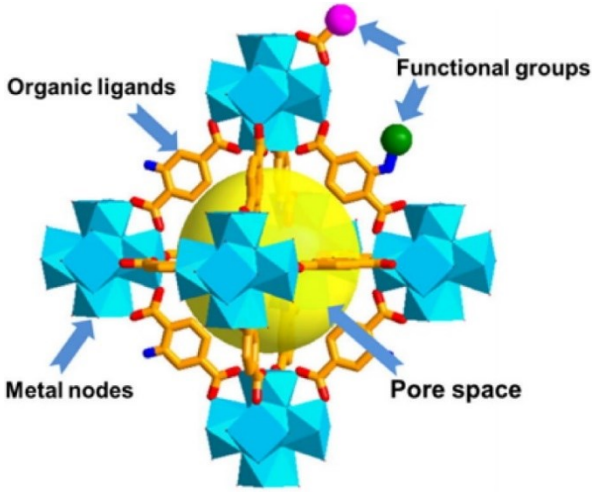

Figure 1.7 Illustration for the construction elements of functional MOFs. Reprinted from Ref.43, Copyright 2019, with permission from Elsevier.

Deng et al. demonstrated that MOFs are able to accommodate multiple functional groups within its structure by mixing the linker.[44] They found that by making a multivariate of MOF-5, a single phase containing up to 8 distinct functionalities allowed for enhanced properties. To synthesise this material, they started with 1,4-benzenedicarboxylate and its derivatives, all having the same length. After comparing the H_2 storage capacity of MOF-5 with other variates, they found that the latter had much better uptake capacity.[44]

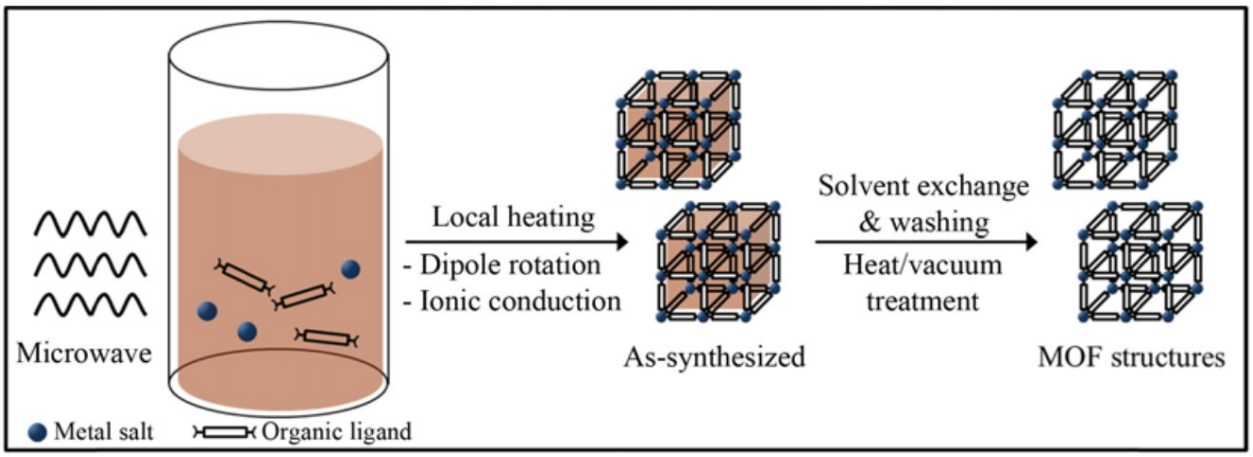

Figure 1.8 Microwave-assisted solvothermal synthesis of MOF structures. From Ref.45, Reproduced with permission from Springer Nature.

These useful structures are most often synthesised solvothermally (Fig. 1.9) or by microwave synthesis (Fig. 1.8).[45] Because of the simplicity of solvothermal synthesis, it is most often used to form MOFs.

Horiuchi et al. used a solvothermal method to synthesise a visible light-responsive MOF.[46] They combined the reagents and DMF in a Teflon lined autoclave before mixing for 48 hr at 423 K before collecting and drying the resulting precipitate. The MOF, Ti-MOF-NH_2, was found to be efficient in photocatalyzing hydrogen production when in a triethanolamine (TEOA) containing aqueous solution.[46]

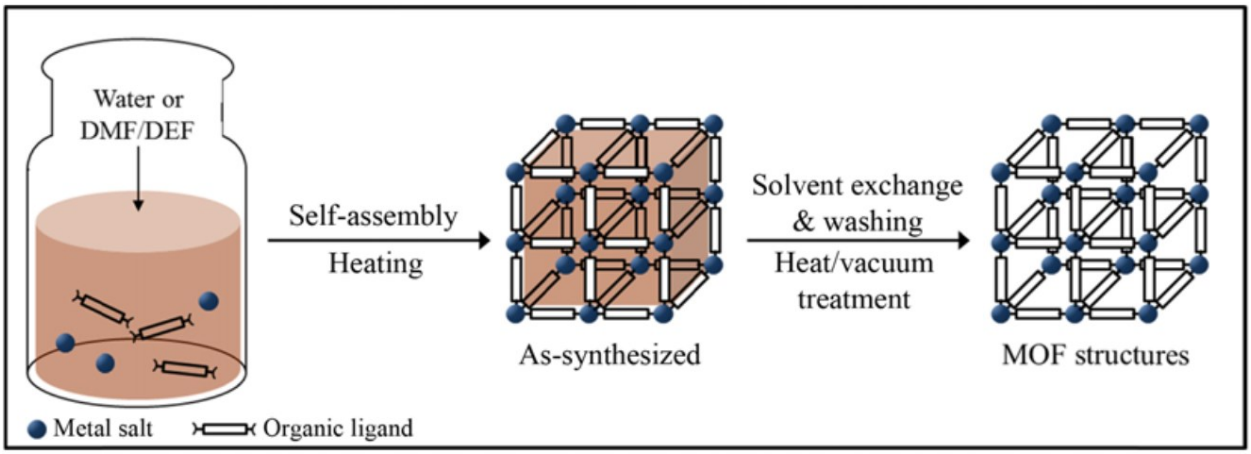

Figure 1.9 Conventional solvothermal synthesis of MOF structures. From Ref.45, Reproduced with permission from Springer Nature.

Unfortunately, the use of solvent in the synthesis of these structures can sometimes be detrimental. Solvent particles tend to stay in the structure, causing it to collapse when attempting to remove them.[47]

Because of this, the mechanochemical synthesis of MOFs has been a point of interest for researchers. Klimakow et al. used a LAG synthesis to form HKUST-1 and MOF-14.[47] Combining the reagents copper acetate monohydrate, H_3BTC and H_3BTB formed a powder then characterised by PXRD, Raman spectroscopy, SEM and differential thermal analysis (DTA). [47] After analysis, the mechanochemically synthesised MOFs were found to be comparable to their solvothermally synthesised counterparts.

MOFs are usually analysed through diffraction-based techniques. MOFs have been notoriously hard to image because of their tendency to collapse and change structure under a transmission electron microscope (TEM). To counteract this damage, Wiktor et al. used Cryo-TEM, a technique using liquid nitrogen to prevent knock-on damage caused by an intense electron beam, to image MOF-5.[48] They first synthesised the cluster, a basic zinc benzoate which was then combined in DMF with the linker. They then drop casted the solution on a clean TEM grid before imaging at

low dose. They found cubic MOF-5 merged particles at around 55nm in size. Using Cryo-TEM allowed for the imaging of the pore structure of nanosized MOF-5 with the most intact structure being analysed along the [100] axis.[48] This did not, however, give images of optimal resolution, indicating the need for further development.

1.5 Defects

Crystalline materials, such as NPs and MOFs, are subject to defects within their lattice. Often time, the best way to find defects in a sample is to use HR-TEM. With a TEM image at such a resolution, a fast Fourier transform (FFT) image of the sample can be performed, which helps to look at the crystallinity of a sample (Fig. 1.10). FFT images of polycrystalline particles have a diffraction pattern with many diffraction spots around the centre of the image. A single crystal will have few diffraction spots with the distance between the spots and the middle representing the reciprocal of the d-spacing. Some researchers want to avoid defects while others prefer them because of the material properties they affect. That is why there has been research aimed at understanding the origins of said crystalline defects.

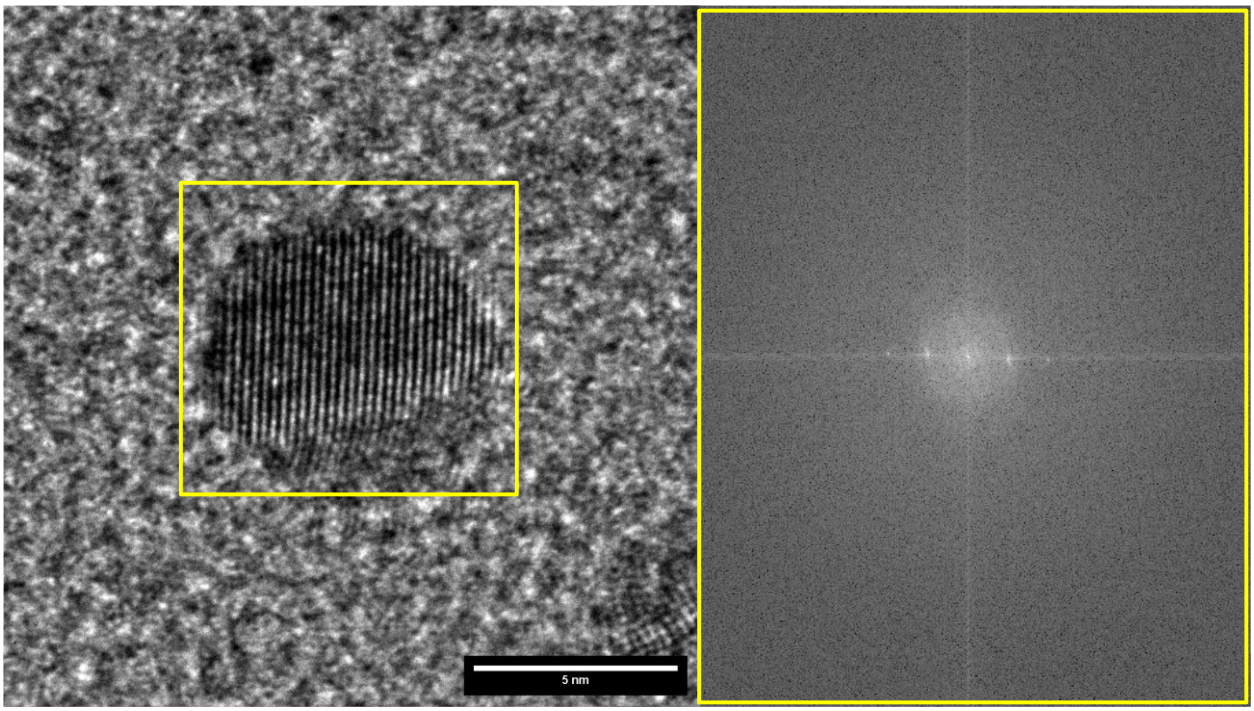

Figure 1.10 Single crystalline DODE capped AuNP aged for 14 days and its FFT image (yellow square).

Defects can be categorised in the following groups; point defects, line defects, two-dimensional defects and three-dimensional defects.[49] Such defects can have multiple effects on a sample which can range from observing a different diffraction pattern than that of the pure sample[50] to a higher conductivity of the particle.[51] The first is usually observed by an impurity in the system while the second is usually a dislocation in the system. Point defects can be formed by irradiation, mechanical formation, alloying or thermal equilibrium depending on the nature of the material.[49] Point defects have a tendency to cluster, which can be attributed to the fact that the formation energy of multiple point defects is smaller than that of the energy sum of each defect.[49]

Stacking faults, grain boundaries and twinning are all examples of two-dimensional defects. Twinning defects are considered common and are usually assigned the term annealing twins; where the growth of one grain at the expense of another.[52] Particles that come in contact along the twin symmetry plane, can also form twinning particles named contact twins.[52] Ou et al. observed the

optical and magnetic properties of specially synthesised twinned crystal structure of $Cu_{2-x}Eu_xO$.[53] After synthesising the material through a gas to liquid method before analysing the sample by x-ray diffraction (XRD), X-ray photoelectron spectroscopy (XPS), field emission scanning electron microscopy (FE-SEM) and TEM (Fig. 1.11).

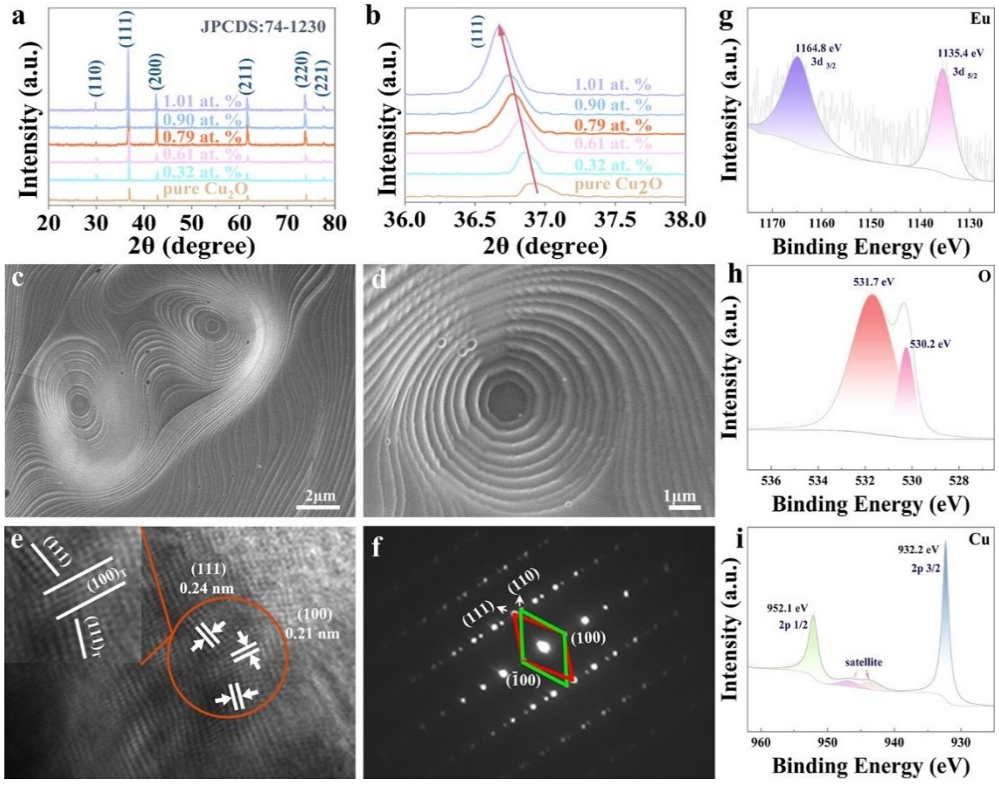

Figure 1.11 (a) XRD for the twinned crystal Cu2O and Cu2–xEuxO bulks with different Eu3+ dopant concentrations. (b) Peaks of all of the samples correspond to the (111) plane. (c, d) SEM images of Cu2–xEuxO (0.79 at. %). (e) HR-TEM and (f) SAED images of the twinned crystal $Cu_{2-x}Eu_xO$ (x= 0.79 at. %) sample. XPS spectra of $Cu_{2-x}Eu_xO$ (0.79 at.%): (g) Eu 3d, (h) O 1s, and (i) Cu 2p. Reprinted with permission from Ref. 53. Copyright 2024 American Chemical Society..

UV-vis absorption spectroscopy and a vibrating sample magnetometer were also both used to analyse optical and magnetic properties.[53] After Eu^{3+} doping, the material became ferromagnetic with the saturation magnetisation decreasing as the doping concentration is increased after a brief initial increase. The twinned material also demonstrated an increase in its absorption capacity when compared to a single crystalline sample.[53]

Oliveira et al. researched the properties of twinned (111) solidified solar grade silicon. [54] After confirming that their particles were twinned by HR-TEM, they analysed the sample by calibrated photoluminescence imaging and light beam induced current. Through these methods, they concluded that their electrical capacitance increased when the twinning order within the particle increased.[54]

1.6 Mechanochemistry - Large scale

The mechanochemical transformations discussed so far have been typically developed using small ball mills, at scales ranging from 100 mg to 10 g. While mechanochemistry has seen some rapid advancement under such conditions, the development of this technique at larger scales (typically beyond 100g) has been less reported. The extruder, Simoloyer and eccentric mill are the only three mechanochemical devices that have been suggested for the largest scale of reactions (<10 kg).[55] Unfortunately, that also means that there is little opportunity for mechanochemistry to be used in a manufacturing process.[55] Some of the problems that researchers encounter include temperature control within the milling jars and the cleaning method still being reliant on solvents.[55] Another important factor is that mechanochemical synthesis tends to be made in batch, where heat removal can be challenging, impeding the industrial capacity.[56] Using instruments such as twin-screw extrusion (TSE) can allow for effective continuous processing, bypassing some of the issues encountered by batch processing.[56]

Jin et al. developed a 15 g scale synthesis of functional metal-organic frameworks (MOF) using already formed metal-organic frameworks and a functional ligand, in their case, IPA-$_L$-Pro (Fig. 1.12).[57]

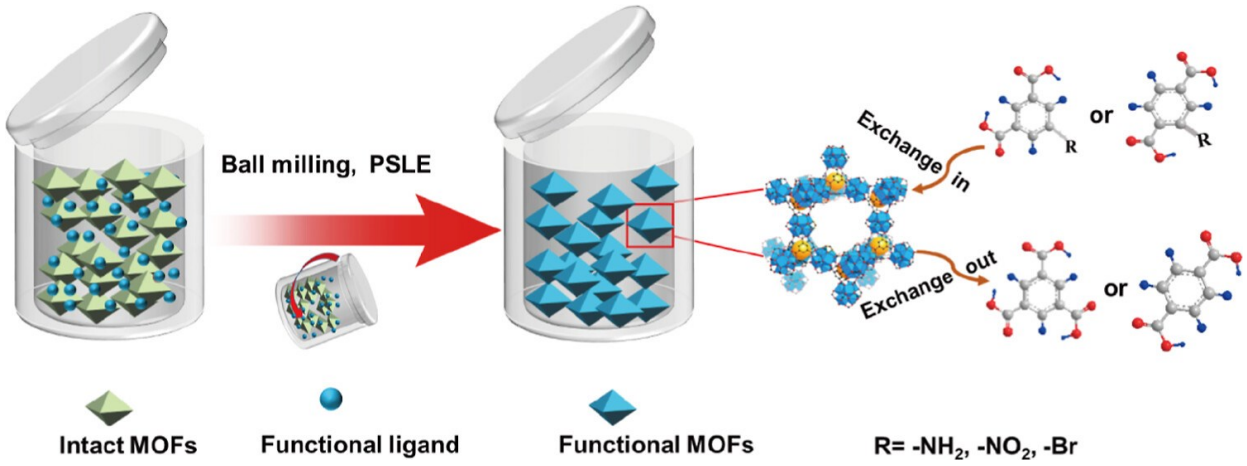

Figure 1.12 Synthetic Scheme of Functional MOFs by the Mechano-PSLE Strategy. Reprinted with permission from Ref. 57. Copyright 2023 American Chemical Society.

After milling both reagents for 30 minutes at 500 rpm, the powder was immersed for 3 days in anhydrous methanol at room temperature. This resulted in 15 grams of chiral functional MOF. They used PXRD to analyse the MOF that they synthesised and compared the spectrum with the one after adding the functional groups. The spectrum showed that the crystallinity of the MOF was not affected by the addition of the functional group. NMR was used to study the ratio of functional group to ligand and SEM images also demonstrated that the morphology of the starting MOFs did not change, with the only visual difference between functional and non-functional MOFs being the colour.[57] Malca et al. reported a one-pot, room-temperature mechanosynthesis of ultrasmall, monodisperse bismuth sulfide nanoparticles (Bi_2S_3 NPs) via ball-milling.[58] The milled or grinded $Bi(NO_3)_3 \cdot 5H_2O$, L-cysteine and either oleyamine (OA) for organic solubility or sodium 6-aminohexanoate (AHA) for aqueous solubility. After 90 minutes of milling and 12 hours of aging, nanoparticles with an average size of 2.09 ± 0.31 nm were observed TEM. However, immediately after milling, the solid material appeared as a yellow paste, and nanoparticles were absent. The self-assembly of nanoparticles was minimally affected by adjusting the milling time or the mechanical activation method. Whether milled for just 5 minutes, ground by hand in a mortar and pestle, or scaled up in a planetary ball mill, similar nanoparticles were consistently produced, with

only slight variations in size. This multi-gram scale and cost-effective approach to synthesizing Bi_2S_3 NPs represents a significant improvement over more time-consuming, high-temperature, and solvent-heavy hydrothermal methods.

1.7 Characterisation

TEM is a specialized imaging technique for ultra-small and ultra-thin specimens that has been widely used by researchers. With its ability to image samples with thicknesses of 200 nm or less, this technique is ideal for crystallinity and structure research because of its various interactions between the electron beam and the sample. The accelerated electrons are emitted from an electron source and go through the sample before scattering at different angles. There are different electron scattering such as elastic and inelastic with the latter indicating energy loss. Those scattered electrons carry a lot of information including structural and chemical, often through inelastic scattering 3.[59] When observing the sample, the contrast can be a great indicator of chemical composition, with metals having a higher contrast than organic materials because of their different density. TEM is able to produce 2D images of the sample which in turn is able to give information such as size and crystallinity by collecting the information provided by the elastic scattered electrons. Unfortunately, researchers have to be mindful when imaging a sample because of the damage such as beam burning, knock-on damage and burning that may occur.[60] Knock on damage is a common damage type seen in TEM imaging because of the electron-nucleus scattering.[61] Figure 1.13 summarizes the different types of damages incurred by samples during a TEM analysis.

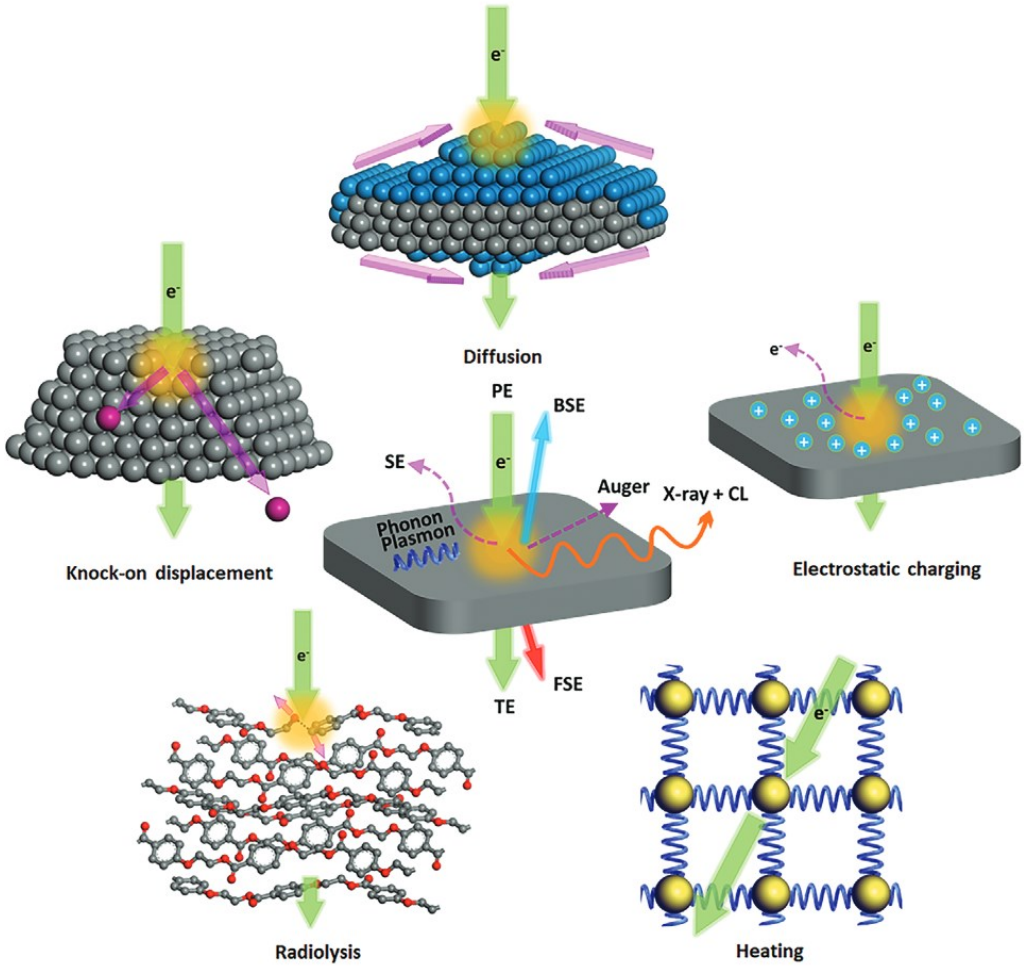

Figure 1.13 Schematic illustration of the interaction between a high-energy electron beam and a thin specimen and associated mechanisms of electron beam damage. PE, SE, TE, FSE, BSE, and CL refer to primary, secondary, transmitted, forward scattering, back scattering and cathodolumi-nescence respectrively. Reproduces from Ref. 59 with permission from Wiley Materials.

Hao et al. used TEM and scanning transmission electron microscopy (STEM), a specialised TEM technique, to look at CeO_2 nanocrystals supported single molecular chain surfactant.[62] STEM scans the sample using a focused electron beam which is able to provide better resolution. Zhang et al. found a way to image sensitive material at the atomic resolution, notably hard to do because of the knock-on damage to the sample from the electron beam.[63] To remedy this, one usually has to reduce the voltage of the electron beam, resulting in lower image resolution. With their developed method, they were able to observe the structure of MOFs and other sensitive material by reduced electron dose, enhance precision alignment and reduced drift. The MOF

imaging results showed both the clusters and ligands clearly, the image being drift corrected and amplitude filtered. They also imaged a hybrid perovskite $CH_3NH_3PbBr_3$ showing ordered nanosized domains with alternating orientation CH_3NH_3 cations, which gives the sample in-plane and out-plane electric dipoles.[63]

Electron energy-loss spectroscopy (EELS) is a technique often combined with STEM that identifies chemical compositions and bonding states of a chosen sample.[64] It does so by analysing the energy lost by electrons in the TEM as they are inelastically scattered.[65] EELS is an alternative to energy dispersive X-Ray spectroscopy (EDX) where the latter is of lower spatial resolution. EELS is able to produce an image map of the elements as they are on the sample using the energy filtering mode, a reproduction of the sample image that has been filtered according to the inelastic electron scattering. It is also able to give a spectrum of energy loss through the spectroscopy mode which acquires a spectrum of energy loss of the scattered electron.[65] This imaging method is versatile and tunable to the researchers' needs and can be used for many applications, especially combined with other methods such as Cryo-STEM.[66]

Ferguson et al. used this technique to demonstrate the considerable mobility of a solid-state sample during aging.[67] The group formed AuNPs using a Turkevich method combining $HAuCl_4 \cdot 3H_2O$, trisodium citrate dihydrate as the reducing agent and ODA as the stabilising ligand. The milling of all three reagents was brief and the resulting yellow powder started aging at room temperature in the dark.[67]

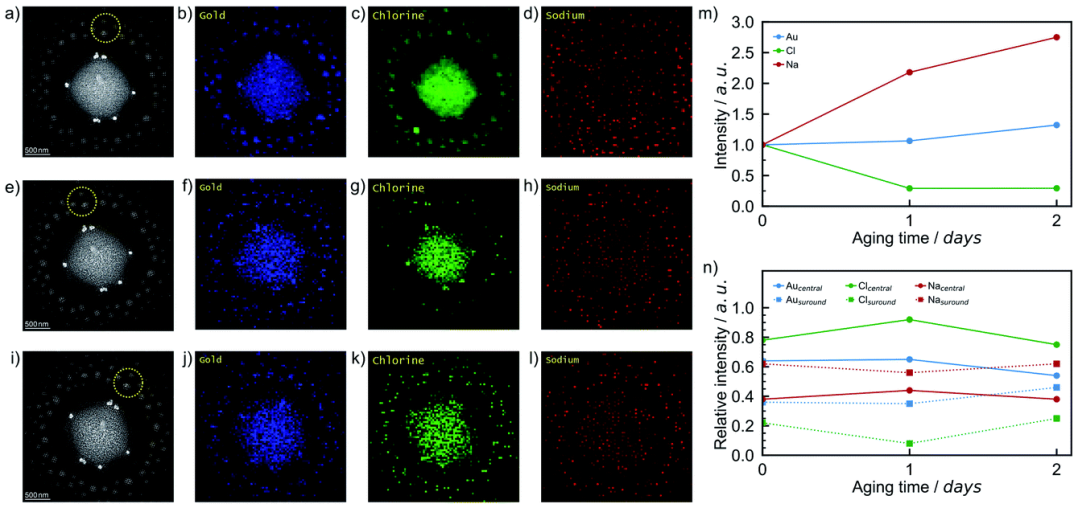

Figure 1.14 STEM-HAADF images and EELS elemental maps for Au, Cl, and Na (left to right, respectively) for freshly milled powder (a–d), after 24 h of aging (e–h), and after 48 h of aging (i–l). In all cases the same particle was studied. The total intensity of each element in the EELS images are given in (m) normalised to the freshly milled powder. The relative EELS intensities for each element over the central particle (solid lines) and its surroundings (dotted lines) are shown in (n). Gold, chlorine, and sodium are represented by blue, green, and red, respectively. Yellow circles (a, e, i) indicate a group of nanoscale particles that we also examined during the aging process. Used with permission of Royal Society of Chemistry , from Ref 67; permission conveyed through Copyright Clearance Center, Inc.

During the 48 hr aging, the sample was analysed by STEM-EELS 3 times (Fig. 1.14). The sample was prepared in the solid state to avoid any solvent influence on the reduction of the gold. Using EELS, spectral images were taken to look into the local distribution of Au, Cl and Na. This allowed for the reduction of gold to be better observed. The spectral images and HAADF micrographs gave the position and relative intensity of the particles and of each element at each imaging time. The group observed the high mobility of all the key elements even with the absence of a solvent.[67]

This introduction, with a focus on solid-state syntheses, nanoparticles, MOFs and TEM, should have prepared the reader for the following thesis in an adequate manner, allowing for a deeper understanding of the subjects of my two years Master's research.

Chapter 2 will focus on understanding the crystallinity of the solid-state AuNPs synthesized as reported in the literature. This understanding is crucial for a better control of their growth and

functionality. Defects and size are two important parameters researchers look at when synthesising these particles.

The lack of knowledge regarding mobility in solid samples during MOF synthesis hinders the possibility of conducting large-scale mechanochemical synthesis of MOFs. Being able to observe the sample by STEM-EELS would allow for a better understanding on how the clusters and linkers come together and of the defects that form in the structure. This will be presented in chapter 3.

1.8 References

(1) Tan, D.; García, F. Main group mechanochemistry: from curiosity to established protocols. *Chemical Society Reviews* **2019**, *48* (8), 2274-2292. DOI: 10.1039/c7cs00813a (acccessed 2024-08-08T16:17:21).

(2) Cuccu, F.; Luca, L. D.; Delogu, F.; Colacino, E.; Solin, N.; Mocci, R.; Porcheddu, A. Mechanochemistry: New Tools to Navigate the Uncharted Territory of "Impossible" Reactions. *ChemSusChem* **2022/09/07**, *15* (17). DOI: 10.1002/cssc.202200362.

(3) Ardila-Fierro, K. J.; Hernández, J. G. Sustainability Assessment of Mechanochemistry by Using the Twelve Principles of Green Chemistry. *ChemSusChem* **2021**, *14* (10), 2145-2162. DOI: 10.1002/cssc.202100478 MEDLINE.

(4) Crawford, D. E.; Wright, L. A.; James, S. L.; Abbott, A. P. Efficient continuous synthesis of high purity deep eutectic solvents by twin screw extrusion. *Chemical Communications* **2016**, *52* (22), 4215-4218. DOI: 10.1039/c5cc09685e (acccessed 2024-09-13T19:36:52).

(5) Fiss, B. G.; Richard, A. J.; Douglas, G.; Kojic, M.; Friscic, T.; Moores, A. Mechanochemical methods for the transfer of electrons and exchange of ions: inorganic reactivity from nanoparticles to organometallics. *Chem Soc Rev* **2021**, *50* (14), 8279-8318. DOI: 10.1039/d0cs00918k From NLM PubMed-not-MEDLINE.

(6) D'Amato, R.; Bondi, R.; Moghdad, I.; Marmottini, F.; McPherson, M. J.; Naïli, H.; Taddei, M.; Costantino, F. "Shake 'n Bake" Route to Functionalized Zr-UiO-66 Metal–Organic Frameworks. *Inorganic Chemistry* **2021**, *60* (18), 14294-14301. DOI: 10.1021/acs.inorgchem.1c01839.

(7) Singh, N. K.; Hardi, M.; Balema, V. P. Mechanochemical synthesis of an yttrium based metal–organic framework. *Chemical Communications* **2013**, *49* (10), 972-974, 10.1039/C2CC36325A. DOI: 10.1039/C2CC36325A.

(8) Užarević, K.; Wang, T. C.; Moon, S.-Y.; Fidelli, A. M.; Hupp, J. T.; Farha, O. K.; Friščić, T. Mechanochemical and solvent-free assembly of zirconium-based metal–organic frameworks. *Chemical Communications* **2016**, *52* (10), 2133-2136. DOI: 10.1039/c5cc08972g (acccessed 2024-06-03T19:42:59).

(9) Rak, M. J.; Saadé, N. K.; Friščić, T.; Moores, A. Mechanosynthesis of ultra-small monodisperse amine-stabilized gold nanoparticles with controllable size. *Green Chem.* **2014**, *16* (1), 86-89. DOI: 10.1039/c3gc41827h.

(10) Chen, Y.; Soler, L.; Xie, C.; Vendrell, X.; Serafin, J.; Crespo, D.; Llorca, J. A straightforward method to prepare supported Au clusters by mechanochemistry and its application in photocatalysis. *Applied Materials Today* **2020**, *21*, 100873. DOI: 10.1016/j.apmt.2020.100873 (acccessed 2024-06-18T20:33:38).
(11) Mechanochemical solid state synthesis of (Cd0.8Zn0.2)S quantum dots: Microstructure and optical characterizations. *Journal of Alloys and Compounds* **2011/03/10**, *509* (10). DOI: 10.1016/j.jallcom.2011.01.035.
(12) Synthesis and characterization of Zn1-xAcxS (0≤x≤0.1) nanocrystalline quantum dots prepared via soft mechanochemical approach. *Ceramics International* **2019/11/01**, *45* (16). DOI: 10.1016/j.ceramint.2019.07.082.
(13) Friščić, T. New opportunities for materials synthesis using mechanochemistry. *Journal of Materials Chemistry* **2010**, *20* (36). DOI: 10.1039/c0jm00872a.
(14) Dachille, F.; Roy, R. High-pressure Phase Transformations in Laboratory Mechanical Mixers and Mortars. *Nature* **1960**, *186* (4718), 34-34. DOI: 10.1038/186034a0.
(15) Treece, R. E.; Macala, G. S.; Kaner, R. B. Rapid synthesis of gallium phosphide and gallium arsenide from solid-state precursors. *Chemistry of Materials* **1992**, *4*, 9-11.
(16) Patil, A. O.; Curtin, D. Y.; Paul, I. C. Solid-state formation of quinhydrones from their components. Use of solid-solid reactions to prepare compounds not accessible from solution. *Journal of the American Chemical Society* **1984**, *106* (2), 348-353. DOI: 10.1021/ja00314a017.
(17) *Retsch, LABORATORY MILLS, GRINDERS & CRUSHERS for primary and fine size reduction*. https://www.retsch.com/products/milling/mortar-grinders/rm-200/ (accessed.
(18) Cliffe, M. J.; Mottillo, C.; Stein, R. S.; Bučar, D.-K.; Friščić, T. Accelerated aging: a low energy, solvent-free alternative to solvothermal and mechanochemical synthesis of metal–organic materials. *Chemical Science* **2012**, *3* (8), 2495-2500. DOI: 10.1039/c2sc20344h (acccessed 2023-05-16T14:51:53).
(19) Štrukil, V. Highly Efficient Solid-State Hydrolysis of Waste Polyethylene Terephthalate by Mechanochemical Milling and Vapor-Assisted Aging. *ChemSusChem* **2021**, *14* (1), 330-338. DOI: 10.1002/cssc.202002124 (acccessed 2024-08-08T16:03:31).
(20) Michalchuk, A. A. L.; Tumanov, I. A.; Boldyreva, E. V. Ball size or ball mass – what matters in organic mechanochemical synthesis? *CrystEngComm* **2019**, *21* (13), 2174-2179. DOI: 10.1039/c8ce02109k (acccessed 2024-08-28T17:57:32).
(21) Fischer, F.; Fendel, N.; Greiser, S.; Rademann, K.; Emmerling, F. Impact Is Important—Systematic Investigation of the Influence of Milling Balls in Mechanochemical Reactions. *Organic Process Research & Development* **March 27, 2017**, *21* (4). DOI: 10.1021/acs.oprd.6b00435.
(22) Richard, A. J.; Ferguson, M.; Fiss, B. G.; Titi, H. M.; Valdez, J.; Provatas, N.; Friščić, T.; Moores, A. In situ study of Au nanoparticle formation in a mechanochemical-aging-based method. *Nanoscale Advances* **2023**, *5* (10), 2776-2784. DOI: 10.1039/d2na00759b (acccessed 2023-05-31T16:15:33).
(23) Adams, C. J.; Colquhoun, H. M.; Crawford, P. C.; Lusi, M.; Orpen, A. G. Solid-state interconversions of coordination networks and hydrogen-bonded salts. *Angew Chem Int Ed Engl* **2007**, *46* (7), 1124-1128. DOI: 10.1002/anie.200603593 From NLM PubMed-not-MEDLINE.
(24) Chen, L.; Regan, M.; Mack, J. The Choice Is Yours: Using Liquid-Assisted Grinding To Choose between Products in the Palladium-Catalyzed Dimerization of Terminal Alkynes. *ACS Catalysis* **January 6, 2016**, *6* (2). DOI: 10.1021/acscatal.5b02001.
(25) Friscic, T.; Reid, D. G.; Halasz, I.; Stein, R. S.; Dinnebier, R. E.; Duer, M. J. Ion- and liquid-assisted grinding: improved mechanochemical synthesis of metal-organic frameworks reveals salt inclusion and anion templating. *Angew Chem Int Ed Engl* **2010**, *49* (4), 712-715. DOI: 10.1002/anie.200906583 From NLM Medline.

(26) Yang, J.; Feng, X.; Lu, G.; Li, Y.; Mao, C.; Wen, Z.; Yuan, W. NaCl as a solid solvent to assist the mechanochemical synthesis and post-synthesis of hierarchical porous MOFs with high I₂vapour uptake. *Dalton Transactions* **2018**, *47* (14), 5065-5071. DOI: 10.1039/c8dt00339d.
(27) Pentecost, A.; Gour, S.; Mochalin, V.; Knoke, I.; Gogotsi, Y. Deaggregation of Nanodiamond Powders Using Salt- and Sugar-Assisted Milling. **November 2, 2010**. DOI: 10.1021/am100720.
(28) Do, J.-L.; Mottillo, C.; Tan, D.; Štrukil, V.; Friščić, T. Mechanochemical Ruthenium-Catalyzed Olefin Metathesis. *Journal of the American Chemical Society* **February 12, 2015**, *137* (7). DOI: 10.1021/jacs.5b00151.
(29) Krupinski, P.; Kornowicz, A.; Sokolowski, K.; Cieslak, A. M.; Lewinski, J. Applying Mechanochemistry for Bottom-Up Synthesis and Host-Guest Surface Modification of Semiconducting Nanocrystals: A Case of Water-Soluble beta-Cyclodextrin-Coated Zinc Oxide. *Chemistry* **2016**, *22* (23), 7817-7823. DOI: 10.1002/chem.201600182 From NLM Medline.
(30) Moores, A. Bottom up, solid-phase syntheses of inorganic nanomaterials by mechanochemistry and aging. *Current Opinion in Green and Sustainable Chemistry* **2018**, *12*, 33-37. DOI: 10.1016/j.cogsc.2018.05.004.
(31) Lin, Y.; Watson, K. A.; Ghose, S.; Smith, J. G.; Williams, T. V.; Crooks, R. E.; Cao, W.; Connell, J. W. Direct Mechanochemical Formation of Metal Nanoparticles on Carbon Nanotubes. *The Journal of Physical Chemistry C* **2009**, *113* (33), 14858-14862. DOI: 10.1021/jp905076u (acccessed 2022-11-02T17:24:30).
(32) Konishi, Y.; Kadota, K.; Tozuka, Y.; Shimosaka, A.; Shirakawa, Y. Amorphization and radical formation of cystine particles by a mechanochemical process analyzed using DEM simulation. *Powder Technology* **2016**, *301*, 220-227. DOI: 10.1016/j.powtec.2016.06.010.
(33) Lin, X.; Liang, Y.; Lu, Z.; Lou, H.; Zhang, X.; Liu, S.; Zheng, B.; Liu, R.; Fu, R.; Wu, D. Mechanochemistry: A Green, Activation-Free and Top-Down Strategy to High-Surface-Area Carbon Materials. *ACS Sustainable Chemistry & Engineering* **September 15, 2017**, *5* (10). DOI: 10.1021/acssuschemeng.7b02462.
(34) Haruta, M. Size- and support-dependency in the catalysis of gold. *Catalysis Today* **1997**, *36* (1), 153-166. DOI: https://doi.org/10.1016/S0920-5861(96)00208-8.
(35) Bond, G. C.; Thompson, D. T. Gold-catalysed oxidation of carbon monoxide. *Gold Bulletin* **2000**, *33* (2), 41-50. DOI: 10.1007/bf03216579 (acccessed 2024-08-22T22:04:57).
(36) Daniel, M.-C.; Astruc, D. Gold Nanoparticles: Assembly, Supramolecular Chemistry, Quantum-Size-Related Properties, and Applications toward Biology, Catalysis, and Nanotechnology. *Chemical Reviews* **2004**, *104* (1), 293-346. DOI: 10.1021/cr030698+.
(37) Wu, Y.; Ali, M. R. K.; Chen, K.; Fang, N.; El-Sayed, M. A. Gold nanoparticles in biological optical imaging. *Nano Today* **2019**, *24*, 120-140. DOI: https://doi.org/10.1016/j.nantod.2018.12.006.
(38) Ali, H. S.; El-Haj, B. M.; Saifullah, S.; Kawish, M. Chapter 4 - Gold nanoparticles in cancer diagnosis and therapy. In *Metal Nanoparticles for Drug Delivery and Diagnostic Applications*, Shah, M. R., Imran, M., Ullah, S. Eds.; Elsevier, 2020; pp 43-58.
(39) Anu Mary Ealia, S.; Saravanakumar, M. P. A review on the classification, characterisation, synthesis of nanoparticles and their application. *IOP Conference Series: Materials Science and Engineering* **2017**, *263*, 032019. DOI: 10.1088/1757-899x/263/3/032019 (acccessed 2024-02-26T16:49:51).
(40) Debnath, D.; Kim, S. H.; Geckeler, K. E. The first solid-phase route to fabricate and size-tune gold nanoparticles at room temperature. *Journal of Materials Chemistry* **2009**, *19* (46). DOI: 10.1039/b905260g.

(41) Furukawa, H.; Cordova, K. E.; O'Keeffe, M.; Yaghi, O. M. The chemistry and applications of metal-organic frameworks. *Science (New York, N.Y.)* **2013**, *341* (6149), 1230444. DOI: 10.1126/science.1230444 MEDLINE.
(42) Yusuf, V. F.; Malek, N. I.; Kailasa, S. K. Review on Metal–Organic Framework Classification, Synthetic Approaches, and Influencing Factors: Applications in Energy, Drug Delivery, and Wastewater Treatment. *ACS Omega* **2022**, *7* (49), 44507-44531. DOI: 10.1021/acsomega.2c05310.
(43) Jiao, L.; Seow, J. Y. R.; Skinner, W. S.; Wang, Z. U.; Jiang, H.-L. Metal–organic frameworks: Structures and functional applications. *Materials Today* **2019**, *27*, 43-68. DOI: https://doi.org/10.1016/j.mattod.2018.10.038.
(44) Deng, H.; Doonan, C. J.; Furukawa, H.; Ferreira, R. B.; Towne, J.; Knobler, C. B.; Wang, B.; Yaghi, O. M. Multiple Functional Groups of Varying Ratios in Metal-Organic Frameworks. *Science* **2010**, *327* (5967), 846-850. Life Sciences.
(45) Lee, Y.-R.; Kim, J.; Ahn, W.-S. Synthesis of metal-organic frameworks: A mini review. *Korean Journal of Chemical Engineering* **2013**, *30* (9), 1667-1680. DOI: 10.1007/s11814-013-0140-6 (acccessed 2024-09-12T16:58:18).
(46) Horiuchi, Y.; Toyao, T.; Saito, M.; Mochizuki, K.; Iwata, M.; Higashimura, H.; Anpo, M.; Matsuoka, M. Visible-Light-Promoted Photocatalytic Hydrogen Production by Using an Amino-Functionalized Ti(IV) Metal–Organic Framework. *The Journal of Physical Chemistry C* **September 24, 2012**, *116* (39). DOI: 10.1021/jp3046005.
(47) Klimakow, M.; Klobes, P.; Thünemann, A. F.; Rademann, K.; Emmerling, F. Mechanochemical Synthesis of Metal−Organic Frameworks: A Fast and Facile Approach toward Quantitative Yields and High Specific Surface Areas. *Chemistry of Materials* **2010**, *22* (18), 5216-5221. DOI: 10.1021/cm1012119 (acccessed 2023-05-02T17:23:54).
(48) Wiktor, C.; Turner, S.; Zacher, D.; Fischer, R. A.; Tendeloo, G. V. Imaging of intact MOF-5 nanocrystals by advanced TEM at liquid nitrogen temperature. *Microporous and Mesoporous Materials* **2012**, *162*, 131-135. DOI: https://doi.org/10.1016/j.micromeso.2012.06.014.
(49) Bollmann, W. *Crystal Defects and Crystalline Interfaces*; Springer Berlin Heidelberg, 2012.
(50) Berliner, R.; Werner, S. A. Effect of stacking faults on diffraction: The structure of lithium metal. *Physical Review B* **1986-09-15**, *34* (6). DOI: 10.1103/PhysRevB.34.3586.
(51) Tang, Y.; Ouyang, M. Tailoring properties and functionalities of metal nanoparticles through crystallinity engineering. *Nature Materials* **2007**, *6* (10), 754-759. DOI: 10.1038/nmat1982 (acccessed 2024-02-26T19:09:06).
(52) Cahn, R. Twinned crystals. *Advances in Physics* **1954**, *3* (12), 363-445.
(53) Ou, P.; Wu, M.; Tong, H.; Zhang, Z.; Zhang, K.; Chuai, M.; Chai, G.-L. Doping Concentration Regulates the Optical and Magnetic Properties of Twinned Crystal Cu2–xEuxO. *Crystal Growth & Design* **April 16, 2024**, *24* (9). DOI: 10.1021/acs.cgd.4c00404.
(54) Oliveira, V.; Marie, B.; Cayron, C.; Marinova, M.; Tsoutsouva, M.; Sio, H.; Lafford, T.; Baruchel, J.; Audoit, G.; Grenier, A. Formation mechanism and properties of twinned structures in (111) seeded directionally solidified solar grade silicon. *Acta Materialia* **2016**, *121*, 24-36. DOI: https://doi.org/10.1016/j.actamat.2016.08.063.
(55) Reynes, J. F.; Isoni, V.; García, F. Tinkering with mechanochemical tools for scale up. *Angewandte Chemie International Edition* **2023**, *62* (44), e202300819.
(56) Nicolas Fantozzi; Jean-Noël Volle; Andrea Porcheddu; David Virieux; Felipe García; Evelina Colacino; Nicolas Fantozzi; Jean-Noël Volle; Andrea Porcheddu; David Virieux; et al. Green metrics in mechanochemistry. *Chemical Society Reviews* **2023/10/02**, *52* (19). DOI: 10.1039/D2CS00997H.
(57) Jin, C.; Shi, S.; Liao, S.; Liu, S.; Xia, S.; Luo, Y.; Wang, S.; Wang, H.; Chen, C. Post-Synthetic Ligand Exchange by Mechanochemistry: Toward Green, Efficient, and Large-Scale Preparation of

Functional Metal–Organic Frameworks. *Chemistry of Materials* **May 23, 2023**, *35* (11). DOI: 10.1021/acs.chemmater.3c00652.
(58) Malca, M. Y.; Bao, H.; Bastaille, T.; Saadé, N. K.; Kinsella, J. M.; Friščić, T.; Moores, A. Mechanically Activated Solvent-Free Assembly of Ultrasmall Bi2S3 Nanoparticles: A Novel, Simple, and Sustainable Means To Access Chalcogenide Nanoparticles. *Chemistry of Materials* **September 14, 2017**, *29* (18). DOI: 10.1021/acs.chemmater.7b02134.
(59) Chen, Q.; Dwyer, C.; Sheng, G.; Zhu, C.; Li, X.; Zheng, C.; Zhu, Y. Imaging Beam-Sensitive Materials by Electron Microscopy. *Advanced Materials* **2020**, *32* (16), 1907619. DOI: 10.1002/adma.201907619 (acccessed 2024-08-30T15:47:05).
(60) Williams, D. B.; Carter, C. B. The Transmission Electron Microscope. In *Transmission Electron Microscopy*, Springer US, 1996; pp 3-17.
(61) Egerton, R. F. Control of radiation damage in the TEM. *Ultramicroscopy* **2013**, *127*. DOI: 10.1016/j.ultramic.2012.07.006.
(62) Hao, X.; Chen, C.; Saito, M.; Yin, D.; Inoue, K.; Takami, S.; Adschiri, T.; Ikuhara, Y. Direct Imaging for Single Molecular Chain of Surfactant on CeO(2) Nanocrystals. *Small* **2018**, e1801093. DOI: 10.1002/smll.201801093 From NLM Publisher.
(63) Zhang, D.; Zhu, Y.; Liu, L.; Ying, X.; Hsiung, C.-E.; Sougrat, R.; Li, K.; Han, Y. Atomic-resolution transmission electron microscopy of electron beam–sensitive crystalline materials. *Science* **2018**, *359* (6376), 675-679. DOI: 10.1126/science.aao0865 (acccessed 2024-03-15T16:53:54).
(64) Suenaga, K.; Sato, Y.; Liu, Z.; Kataura, H.; Okazaki, T.; Kimoto, K.; Sawada, H.; Sasaki, T.; Omoto, K.; Tomita, T.; et al. Visualizing and identifying single atoms using electron energy-loss spectroscopy with low accelerating voltage. *Nature Chemistry* **2009**, *1* (5), 415-418. DOI: 10.1038/nchem.282 (acccessed 2024-08-23T19:03:55).
(65) Keast, V. J. Application of EELS in Materials Science. *Materials Characterization* **2012**, *73*, 1-7. DOI: 10.1016/j.matchar.2012.07.013.
(66) Hart, J. L.; Cha, J. J. Seeing Quantum Materials with Cryogenic Transmission Electron Microscopy. *Nano Letters* **June 23, 2021**, *21* (13). DOI: 10.1021/acs.nanolett.1c02146.
(67) Ferguson, M.; Richard, A. J.; Valdez, J.; Fiss, B. G.; Titi, H. M.; Provatas, N.; Friščić, T.; Moores, A. Direct observation by high resolution transmission electron microscopy of gold(<scp>iii</scp>) particle transformation during aging reduction reaction. *Faraday Discussions* **2023**, *241*, 278-288. DOI: 10.1039/d2fd00126h (acccessed 2024-02-27T16:44:45).

2 Study of crystal defects formation in gold nanoparticles grown via solid-state aging techniques

After introducing the thesis in chapter 1, chapter 2 explores how solid-state synthesis influences the crystallinity of gold nanoparticles (AuNPs). Building on a previous study that combined gold metal salt, trisodium citrate, and octadecylamine (an 18-carbon linear amine), the effects of varying chain length and temperature on the crystallinity of AuNPs were analyzed. High-resolution transmission electron microscopy and X-ray diffraction were used to image and identify the presence of Au^0 more specifically, their size and lattices. Understanding solid-state synthesis and nanoparticle defects is necessary for this chapter. This chapter presents a detailed characterization and analysis of these AuNPs formed during aging at two different temperatures.

This chapter is based on a submitted article and has been reprinted with permission from all co-authors.

2.1 Abstract

The synthesis of nanoparticles by mechanochemistry opens a new avenue for the greener fabrication of important functional materials. Understanding the mechanism of defect formation in such syntheses is crucial to future discoveries. Gold nanoparticles (AuNPs) were synthesized under mechanochemical and aging conditions, using two different chain length amine capping agents, namely octadecylamine (ODA) and dodecylamine (DODE), each at two different temperatures. The formation of defects was monitored by solid-state sampling transmission electron microscopy for up to 15 days. Our findings indicate that longer amine chains were associated with smaller nanoparticle size, fewer defects and higher crystallinity, particularly at smaller sizes. The shorter chain DODE-capped nanoparticles showed more defects, including single and multiply twinned structures, across a broader range of particle sizes. We interpreted this as the result of the shorter chain's lower molecular inertia creating a more mobile solid system of higher entropy. Higher aging temperatures resulted in increased entropy and a greater variety of crystalline arrangements, observed as more disordered structures. These results highlight the critical role of capping agent selection and aging conditions in tailoring the properties of mechanochemically synthesized nanoparticles for applications in catalysis, materials science, and biotechnology.

2.2 Introduction

Nanomaterials (NMs) are structures with at least one dimension in the nanometer scale, typically ranging from 1 to 100 nanometers. Various materials, including metals, semiconductors, polymers, and biological molecules, have been produced in the nanoscale.[1] Due to their small size and high

surface area-to-volume ratio[2], NMs exhibit unique properties compared to their bulk counterparts. This makes them highly versatile and applicable across a wide range of fields. Gold nanoparticles (AuNPs) have received a particularly high level of attention in terms of research interest and applications[3] such as bioimaging luminescence[4] and catalysis[5]. AuNPs are great tools for biology thanks to their chemical and toxicological inertness, biocompatibility, as well as their optical activity generated through surface plasmon band (SPB) adsorption.[3] They have been exploited for bioassay applications, imaging of cells, biomolecules, and other biological components, as well as photothermal therapies.[3, 6] AuNPs have also gained attention in catalysis, especially fixed onto supporting oxides like Co_3O_4, Fe_2O_3, or TiO_2.[7] They have prior usage in small molecule activation, including CO and H_2 oxidation, NO reduction, water-gas shift reaction, CO_2 hydrogenation, and methanol catalytic combustion, as well as organic transformations.[3]

Since AuNPs have such a variety of uses, researchers usually select their synthesis method based on the desired properties. Chemical reduction is one of the most popular and widely used methods for synthesizing metallic nanoparticles, such as gold, silver, and platinum nanoparticles as grow occurs through a bottom-up approach.[1] Bottom-up synthesis requires three components; a metal precursor (typically a metal salt), a reducing agent and a capping agent. The capping agent assists and controls NP seeding and growth while the reducing agent drives the reduction of the metal precursor.[8,1] Bottom-up methods can achieve ultrasmall sizes (< 10 nm) which is generally not possible through a top-down method, more often used in large scaler synthesis such as size and shape control.[9] The traditional solvothermal approach offers several advantages, including simplicity, efficiency, cost-effectiveness, and continuous operation with high yields.[1] Whilst is has many advantages it requires a high amount of solvent for an effective synthesis. Mechanochemistry is a method that has gotten more attention for nanoparticle synthesis.[10] As an innovative approach

to chemical transformation, it utilises mechanical energy to drive reactions whilst avoiding the use of bulk solvents.[11] Compared to solvent-based reactions, solid-state reactions may result in enhanced or unique selectivity, higher atom economy, unique products, and improved energy efficiency.[12] Metal-organic frameworks,[13,14,15] nanoparticles,[16] photocatalyst,[17] quantum dots[18,19] and co-crystals[20] are some examples of materials that can be made using mechanochemistry. Mechanochemistry is sometimes complemented by accelerated aging, a reaction condition in which chemical transformations occur through ambient thermal energy in the solid state, with controllable parameters such as temperature[13], movement[21], light[22], humidity[21] and solvent vapour.[23] To utilise these advantages to their maximum potential, it is important to gain insight into the mechanisms of mechanochemical and aging-based transformations.

Mechanochemistry[16, 24] and aging[25] as been demonstrated as being conducive to the formation of size controlled AuNPs. In previous work from our group, an AuNP synthesis was developed through solid-state aging, based on a modified version of the well-known Turkevich reaction.[25] This modification introduced a citrate-induced chemical aging component to the reaction that enabled the in-situ observation, via high-resolution transmission electron microscopy (HR-TEM), of gold reduction, precursors reactivity, and nanoparticle growth over a period of days to weeks.[26] During experimental observations, certain AuNPs exhibited defects in their crystalline structure. Notable among these defects are twinning, stacking faults, and miscellaneous grain boundaries. This work provides a unique opportunity for in-depth characterisation of the mechanochemical and solid-state reactivity kinetics and established that this reaction followed a sigmoidal behavior.

Defects play a key role in nanoparticle reactivity[27] and modulate materials properties such as electrical conductivity and mechanical strength[28] by changing how electrons and phonons propagate through the lattice.[29, 30] Structural and edge defects are particularly impactful, for example, on quantum dots designed for optical and electronic applications.[31] Twinning is a specific type of defect with major impact on magnetic properties, which can also affect a materials potential for superconductivity.[32] A nanoparticle with densely populated twin boundaries can also exhibit significantly higher tensile strength than its pure metal counterpart.[33] A mechanochemical process may prove to be an effective means to experimentally support the modelling of nanoparticle twinning, as it eliminates the impact of solvents on the nanoparticle structure formation and behaviour. It also benefits experimentally as artificially extended reactions allow for a prolonged observation period of crystal growth processes in the solid state.

Herein we adapted our solid-state aging AuNPs synthesis and in-situ characterisation method to track the formation of defects in the crystallinity. For this study we analysed the effect of ligand chain length, as well as the effects of aging temperature on the size of the made NP, the nature of the defects as well as their frequency. Analysis was done via HR-TEM, allowing Fast-Fourier Transform (FFT) images of crystalline and amorphous particles to be compiled and quantified. Powder X-ray diffraction (PXRD) was also used to track the presence of crystalline gold in our samples. This work provides insight into the modulation of crystalline properties in NMs produced in the solid phase, based on energy and mobility parameters.

2.3 Discussion

To study the size and crystallinity of nanoparticles while aging in the solid phase, we used $HAuCl_4 \cdot 3H_2O$ as the gold salt precursor, trisodium citrate dihydrate as the reducing agent, a long chain amine, and sodium chloride (Fig. 2.1). [25]

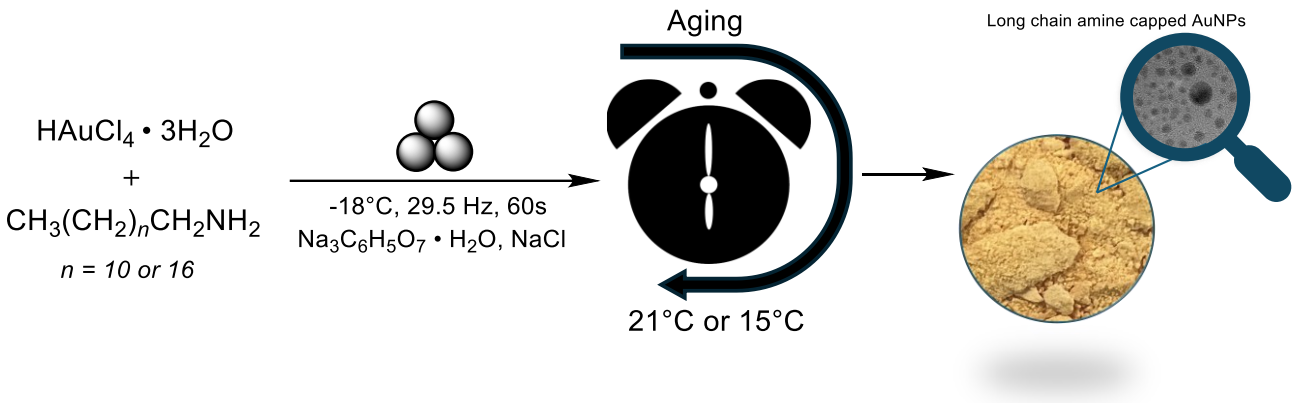

Figure 2.1 Synthesis of long chain amine-capped AuNPs by mechanochemical mixing under frozen conditions, followed by aging at 15 or 21 °C for up to 15 days.

Two different amine chain lengths were explored to investigate the impact of chain length on the nature and frequency of observed crystalline defects. The longer chain, octadecylamine (ODA), consists of 18 linear carbons, while the shorter chain, dodecylamine (DODE), consists of 12 linear carbons. In our reaction, NaCl was used as a solid auxiliary, as it was found that samples containing DODE aggregated during milling, preventing even mixing of the sample.[34] All the reagents were combined with a zirconium ball, frozen at -28 °C for 60 minutes, and ground together in a zirconium milling jar for 60 seconds at 29.5 Hz. Subsequent aging for up to two weeks took place at two different temperatures: 21 °C and 15 °C. The pre-cooling ensured that no AuNPs formed during milling, as demonstrated by our group before,[25] to observe solely the effect of NP growth by aging.

The yellow to orange colour of the gold-salt precursor changed colour during the aging process, taking on the distinctive purple that results from localised SPR effects in AuNPs.[35] The sample containing ODA started as a bright yellow powder, while the DODE sample was initially burnt orange.[35] After 15 days at room temperature, the ODA-capped AuNPs turned purple, with the sample aged at 15 °C, the colour changed much slower than the sample aged at room temperature. As for the DODE-capped AuNPs, the sample turned a purple-blue colour by day 4, only becoming darker as the days progressed.

We first tracked the reaction's progression by PXRD at the same time each day, for 15 days. Using PXRD we monitored the growth of the Au(111) X-ray reflection at $2\theta = 38.2°$[36] to track the growth of AuNPs. Figure 2.2 displays intense peaks corresponding to the NaCl added to the sample before milling, which made the observation of AuNPs peaks difficult.[37].

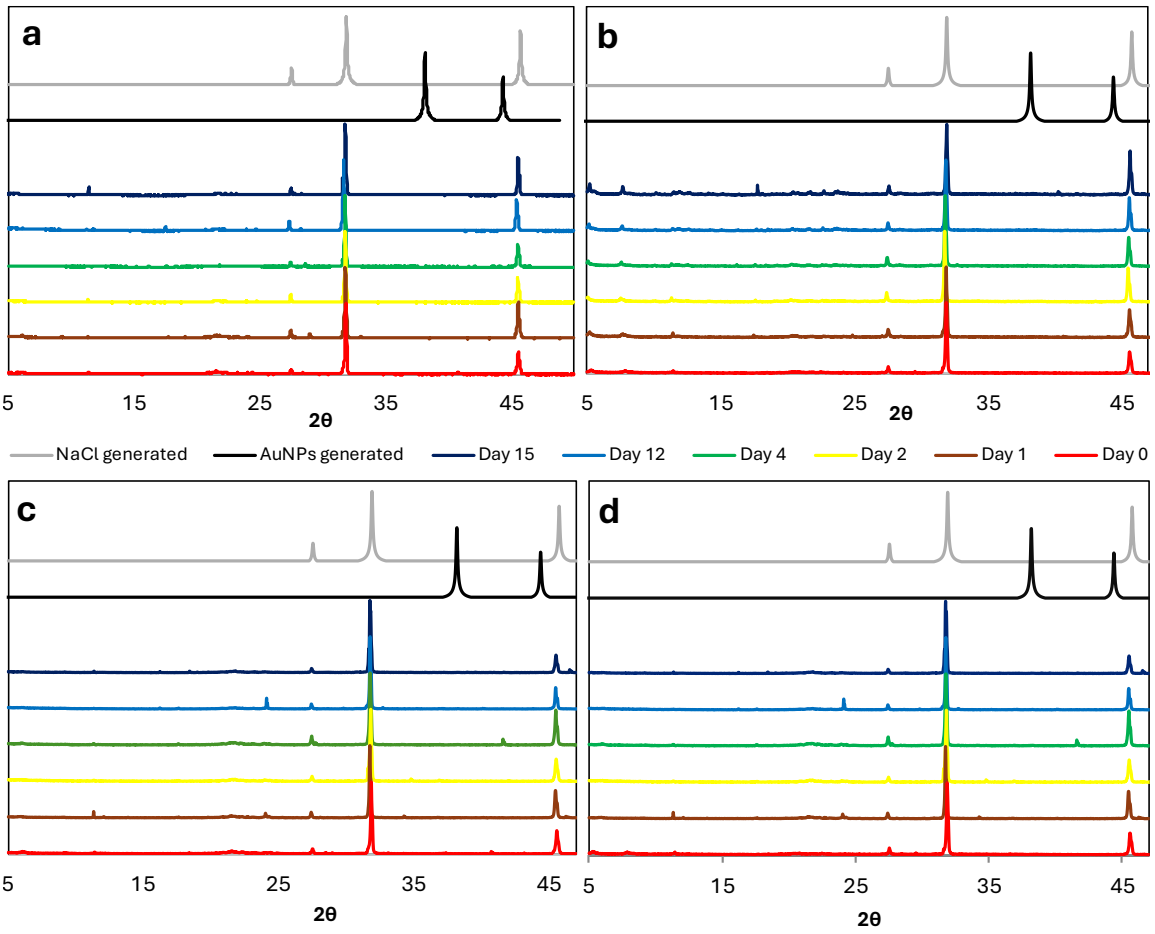

Figure 2.2; XRD spectrum of amine capped AuNPs showing the absence of AuNPs peaks, as generated; a)ODA capped aged at 21°C, b) DODE capped aged at 21°C, c) ODA capped aged at 15°C, d) DODE capped aged at 15°C

We found however that washing samples allowed us to see peaks at $2\theta = 38.2°$ representing the Au(111), for samples aged 9 or 15 days at room temperature. This result confirms the presence of crystalline Au^0 nanoparticles. PXRD however is unable to discern between the kinds of crystalline defects present in the synthesised AuNPs. We thus turned to TEM for in depth, particle by particle analysis.

To eliminate any risk that suspension of the AuNPs in solvent affects particle[25] formation itself, TEM analysis was carried out using a solid-state sampling technique. A small amount of each sample was taken and mounted on a TEM grid. HR-TEM images were taken and treated using FFT to allow a direct analysis of crystalline defects in growing AuNPs. Single crystalline

nanoparticles were frequently observed, along with other AuNPs demonstrating polycrystallinity, notably orientation changes and stacking faults. Defects such as single-twins and multi-twins were individually counted while stacking faults and grain boundaries were combined in one category for clarity and simplicity.

After compiling the nanoparticle sizes from TEM images using ImageJ[38], the next step involved running the statistics through Fityk[39] to generate size distribution functions. On days 0 and 1, some precursor particles larger than 2nm were observed while growing AuNPs are identified as early as day 2 for some samples. Most product particles sizes were around 1-2 nm with the size increasing over the course of the 15 days. For all conditions, slower growth and better size control were observed for the samples aged at colder temperatures. Specifically, at 15 °C, we only see nanoparticles of sizes greater than 2 nm at day 9 and 12 for DODE and ODA respectively, while they start appearing on day 4 at 21 °C. Less thermal energy is consistent with slower growth, which results in a more controlled and more monodisperse growth.

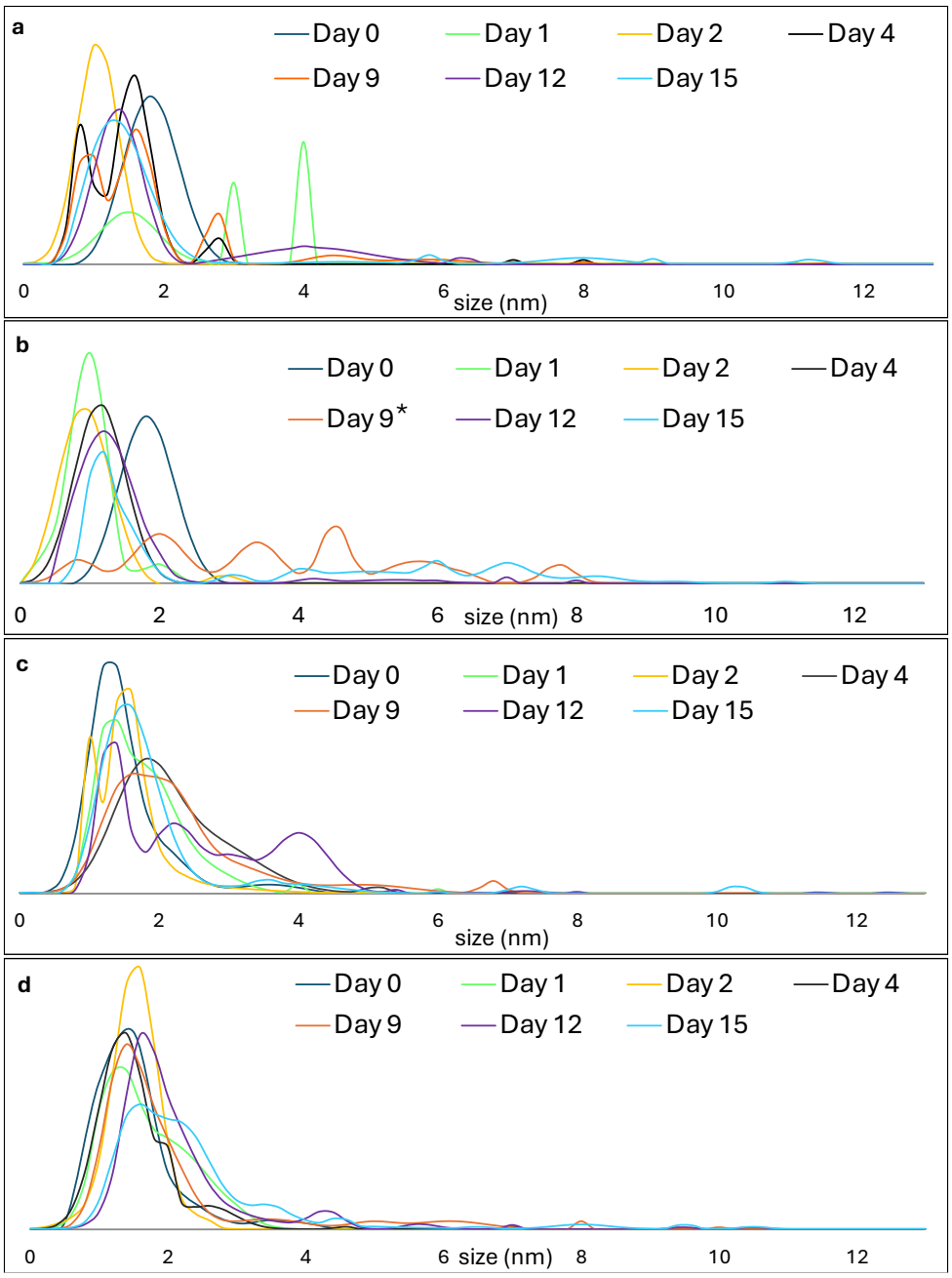

*Figure 2.3; Size of chain amine capped AuNPs over 15 days. a)ODA capped aged at 21°C, b) ODA capped aged at 15°C, c) DODE capped aged at 21°C, d) DODE capped aged at 15°C. *The small number of particles measured reduces the representativeness of the results*

For all conditions, longer aging time led to bigger product particles in the 2 to 8 nm range. For DODE, the shorter chain amine, such large particle appeared sooner in the aging process and were observed more frequently than in other samples. Product particles of sizes above 2 nm were

observed as early as day 2 for DODE while ODA only showed signs of NPs that size at day 9. In short, a shorter chain amine resulted in bigger product particles while a longer chain provided smaller AuNPs. We already observed a similar relationship for the synthesis of long-chain amine based AuNPs made under mechanochemical conditions (ball milling).[16] It was found in this example that a longer chain length created more order around the particle, thus limiting further nanoparticle growth. We propose that a similar effect is at play here.

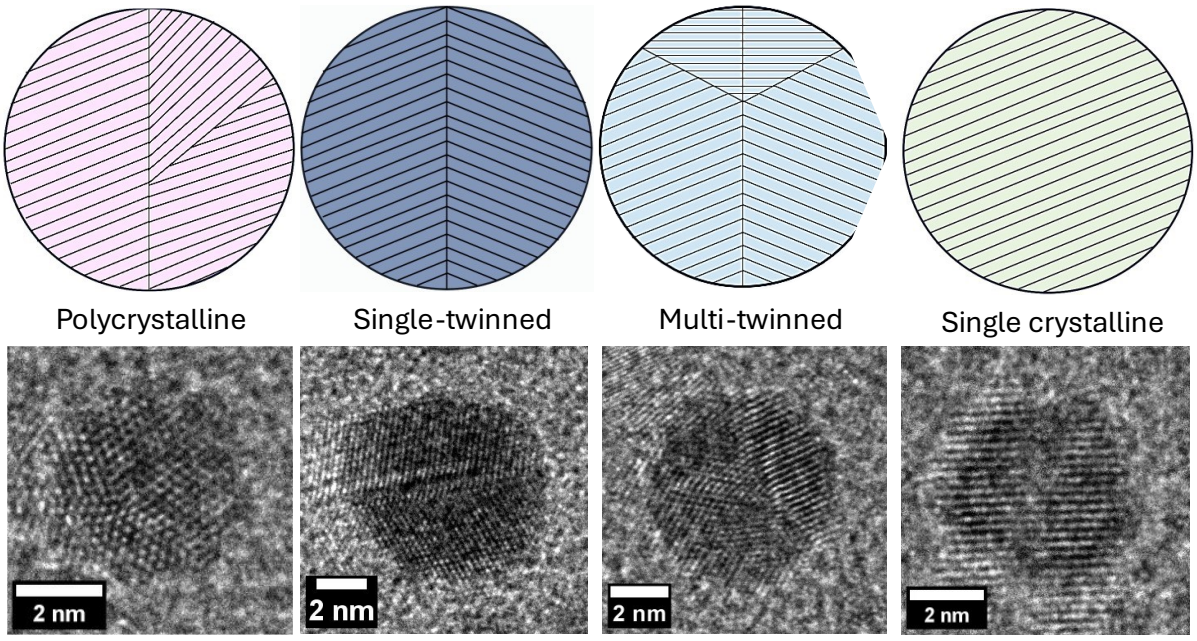

Figure 2.4; Various microstates examples along with TEM images of each.

After compiling the sizes, we used FFT [38] as a tool which allows the treatment of HR-TEM generated images so as to extract crystallinity information. Using ImageJ, we could then classify each particle in terms of their crystallinity property, and bin them as single crystal, single twin, multi twin, polycrystalline and other defects (Figure 2.4). We observed that as the size of the nanoparticle grew, an increase in defects and number of polycrystalline particles was observed, for

both ligands and temperatures tested (Figure 2.5). It is important to note that the 7-8 nm bin was typically less populated, making it less statistically relevant than the other bins.

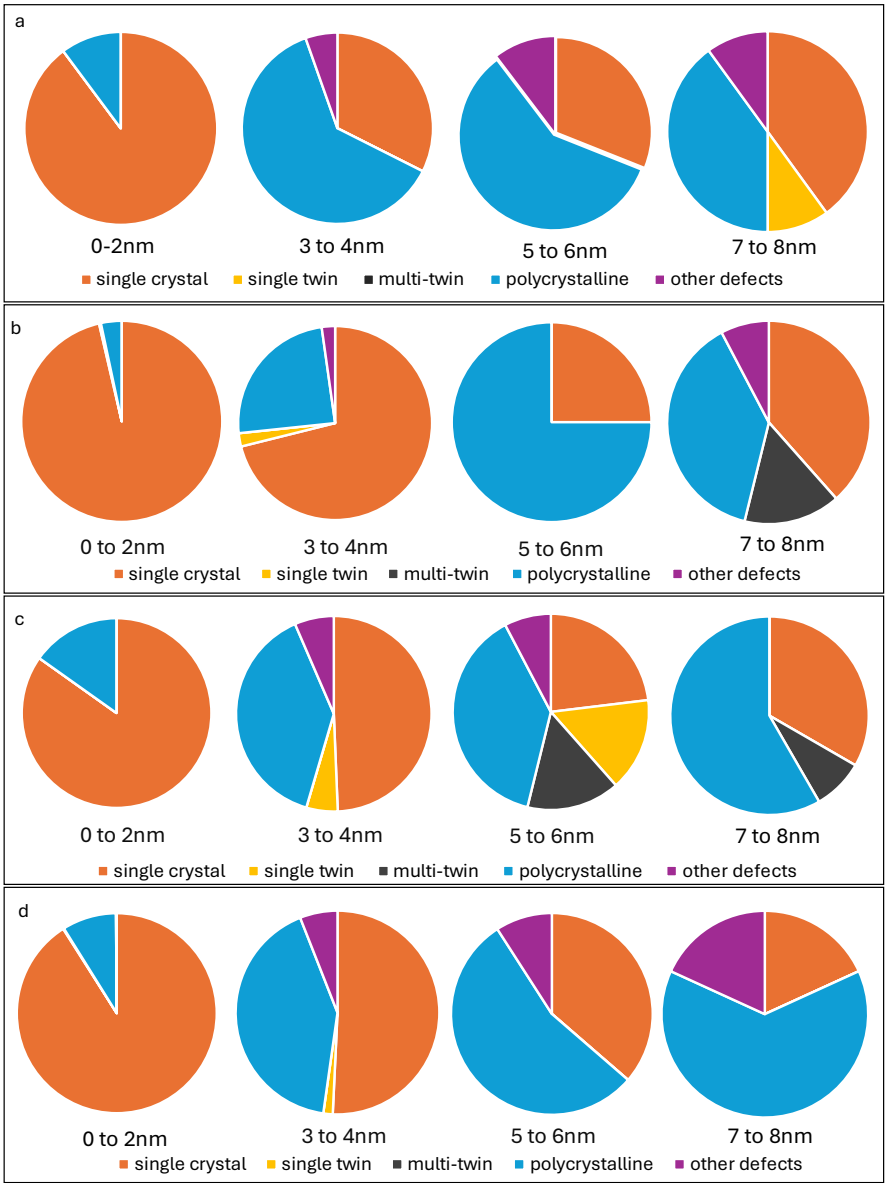

*Figure 2.5; Crystallinity of chain amine capped AuNPs. a)ODA capped aged at 21°C, b) ODA capped aged at 15°C, c) DODE capped aged at 21°C, d) DODE capped aged at 15°C. * Numerical values found in Table S1*

Both the 21 °C and 15 °C aged samples had similar ratios of single and polycrystalline for the smallest size range, namely 0-2 nm, for both ligands (Figure 2.5). From 3 nm and beyond, the chain length began affecting crystallinity in a measurable way. For instance, at 21 °C, we observed

more defects in DODE-capped AuNPs (shorter chain) than in ODA-capped ones (longer chain). The shorter chain amine also showed a wider variety of microstates, with notably both single and multiply twinned nanoparticles present in NPs sizes 3-6 nm for DODE but not for ODA (Figure 2.5 a and c). Another interesting point to note is the rarity of twins in the longer chain amine capped NPs. When comparing 21 °C sample with 15 °C ones, it was found that colder temperatures favoured the formation of more ordered systems (Figure 2.5 b and d). It is evident from the analysis of monocrystal AuNPs, which are more abundant in the colder samples, in all side ranges.

Entropic considerations may help explain the observed change in frequency of single to polycrystalline particles, as well as the relative change in twin defects to other defects as a function of changing reaction conditions. As a measure of a crystal system's disorder, entropy increases through the introduction of defects to single crystals, leading to polycrystallinity. There is thus an inverse relationship between crystallinity and entropy.[40] The observed inverse relationship between temperature and order can be easily explained in this framework: at lower temperature, motion is more limited and a higher order can be seen.[40] Similarly, longer amine chains are associated to higher order than shorter chains, as is well know in the field of surface assembled monolayers. If the surface is covered with ligands that have more order, it will slow the growth of the corresponding particle, an effect consistent with the fact we observed smaller particles with longer chains. Past work from our group on mechanochemical synthesis of AuNPs also pointed to the same mechanism.[16] Also, this will result in less defects in the crystalline arrangement, as incoming new gold atoms will have more time to accommodate the local structure during growth.

2.4 Conclusion

This study explored the synthesis and aging of AuNPs in the absence of solvent, focusing on the impact of amine chain length on nanoparticle size, crystallinity, and defect formation. It was found that AuNPs with a longer chain, exhibited fewer defects and higher crystallinity, especially at smaller sizes. On the other hand, a broader range of sizes was observed for AuNPs capped with DODE, which displayed a higher occurrence of defects, including single and multiply twinned structures. This difference is attributed to the smaller molecular inertia of DODE, which allows more work to be done to the system, thus allowing for greater defect formation. Higher aging temperatures resulted in a greater number of microstates and increased entropy, reflecting more disordered structures. Lower aging temperatures yielded more ordered structures with fewer microstates. These findings emphasize the importance of capping agent selection and aging conditions in controlling nanoparticle properties, which is crucial for applications in catalysis, materials science, and biotechnology.

2.5 Experimental

Trisodium citrate dihydrate (ACS reagent, ≥99.0%), tetrachloroauric(III) acid trihydrate (ACS reagent, ≥49.0% Au basis), and 1-octadecylamine (technical grade, 90%) were obtained from Sigma Aldrich and used without further purification. Dodecylamine, 98%, was obtained from Thermo Scientific Chemicals and used without further purification. Sodium Chloride (Anhydrous) was obtained from ACP chemicals and used without further purification.

ODA capped AuNPs synthesis

Trisodium citrate dihydrate (0.0783 g, 0.2664 mmol), tetrachloroauric(III) acid trihydrate (0.0954 g, 0.2421 mmol), 1-octadecylamine (0.3263 g, 1.211 mmol) and sodium chloride (0.75g, 12.8 mmol) were added to separate jars and frozen for 24 hrs. All four chemicals were then added to a 15 ml zirconia milling jar (Form-Tech Scientific) with an 8 mm (3.0 g) diameter zirconia milling ball. The jar containing the reactants was milled for 1 minute at 29.5 Hz on a Retsch MM400 mixer mill.

The resulting yellow powder was transferred to a jar and sealed with parafilm. This sample preparation was done twice. One sample was aged in an opaque container at room temperature (21 °C) while the other sample was aged in a foil paper covered jar at 15°C.

DODE capped AuNPs synthesis

Trisodium citrate dihydrate (0.0983 g, 0.2664 mmol), tetrachloroauric(III) acid trihydrate (0.1200 g, 0.3041 mmol), dodecylamine (0.2818g, 1.211 mmol) and sodium chloride (0.75 g, 12.8 mmol) were added to separate jars and frozen for 24 hrs. All four chemicals were then added to a 15ml zirconia milling jar (Form-Tech Scientific) with an 8 mm (3.0 g) diameter zirconia milling ball. The jar containing the reactants was milled for 1 minute at 29.5 Hz on a Retsch MM400 mixer mill.

The resulting yellow/orange powder was transferred to a jar and sealed with parafilm. This sample preparation was done twice. One sample was aged in an opaque container at room temperature (21 °C) while the other sample was aged in a foil paper covered jar at 15°C.

Characterisation

The TEM studies were performed using a Thermo Scientific Talos F200X transmission electron microscope equipped with a high-brightness XFEG Schottky source, operated at 200 keV. Images were captured in the high contrast mode. TEM grids were prepared using the solid-state method, where the 400 mesh Cu grid was dipped in the milled powder and any excess powder was removed with a compressed air can. Each samples were analyzed on day: 0, 1, 2, 4, 9, 12 and 15. Individual particles, an average of 688 per sample, were sized using the ImageJ software[38].

Solid-state TEM sampling made very small product particles difficult to analyze due to a high frequency of nanoparticle overlap. Most of the samples, however, contained between 150 and 300 measurable particles, which is considered representative of the sample. On some days, only 8-50 product particles were measurable, the solid-state TEM method making it harder to measure particles due to the heavy overlap of nanoparticles.

PXRD studies were performed using a Bruker D8 Advance diffractometer equipped with a Ni-filtered CuKα (λ = 1.5418 Å) source, 1D LYNXEYE detector, and operating at 40kV and 40 mA. PXRD patterns were obtained in a 2θ range of 5° to 50° with an exposure time of 0.60 s and in increments of 0.02°.

2.6 Acknowledgment

We thank the Natural Science and Engineering Research Council of Canada (NSERC) - Discovery Grant and Discovery Accelerator Supplement, the Canada Foundation for Innovation (CFI), the Centre for Green Chemistry and Catalysis (CGCC), and McGill University for their financial support. We thank Hatem Titi for their contribution to the discussion in the PXRD section of this

paper. We thank the Facility for Electron Microscopy Research (FEMR) of McGill University for help in acquiring electron microscopy data. We thank the MC² facility at McGill University for help in acquiring PXRD data.

2.7 References

(1) Anu Mary Ealia, S.; Saravanakumar, M. P. A review on the classification, characterisation, synthesis of nanoparticles and their application. *IOP Conference Series: Materials Science and Engineering* **2017**, *263*, 032019. DOI: 10.1088/1757-899x/263/3/032019 (acccessed 2024-02-26T16:49:51).
(2) Sharma, J. N.; Pattadar, D. K.; Mainali, B. P.; Zamborini, F. P. Size Determination of Metal Nanoparticles Based on Electrochemically Measured Surface-Area-to-Volume Ratios. *Analytical Chemistry* **2018**, *90* (15), 9308-9314. DOI: 10.1021/acs.analchem.8b01905.
(3) Daniel, M.-C.; Astruc, D. Gold Nanoparticles: Assembly, Supramolecular Chemistry, Quantum-Size-Related Properties, and Applications toward Biology, Catalysis, and Nanotechnology. *Chemical Reviews* **2004**, *104* (1), 293-346. DOI: 10.1021/cr030698+.
(4) Lee, L. C.-C.; Lo, K. K.-W. Shining New Light on Biological Systems: Luminescent Transition Metal Complexes for Bioimaging and Biosensing Applications. *Chemical Reviews* **2024**, *124* (15), 8825-9014. DOI: 10.1021/acs.chemrev.3c00629.
(5) Tanaka, M.; Kiriki, Y.; Kiyohara, N.; Hayashi, M.; Tamang, A.; Nakamura, T.; Vacha, M.; Choi, Y.; Choi, J.; Yoshida, W.; et al. Small Au Nanoparticles Synthesized by Peptide-Based Biomineralization for Catalytic Applications. *ACS Applied Nano Materials* **2024**, *7* (10), 11258-11266. DOI: 10.1021/acsanm.4c00780.
(6) Riley, R. S.; Day, E. S. Gold nanoparticle-mediated photothermal therapy: applications and opportunities for multimodal cancer treatment. *WIREs Nanomedicine and Nanobiotechnology* **2017**, *9* (4), e1449. DOI: 10.1002/wnan.1449 (acccessed 2024-09-09T20:54:47).
(7) Corma, A.; Garcia, H. Supported gold nanoparticles as catalysts for organic reactions. *Chemical Society Reviews* **2008**, *37* (9), 2096. DOI: 10.1039/b707314n (acccessed 2024-09-09T21:09:42).
(8) De Oliveira, P. F. M.; Torresi, R. M.; Emmerling, F.; Camargo, P. H. C. Challenges and opportunities in the bottom-up mechanochemical synthesis of noble metal nanoparticles. *Journal of Materials Chemistry A* **2020**, *8* (32), 16114-16141. DOI: 10.1039/d0ta05183g (acccessed 2024-09-12T14:41:44).
(9) Moores, A. Bottom up, solid-phase syntheses of inorganic nanomaterials by mechanochemistry and aging. *Current Opinion in Green and Sustainable Chemistry* **2018**, *12*, 33-37. DOI: 10.1016/j.cogsc.2018.05.004.
(10) Tsuzuki, T.; McCormick, P. G.; Tsuzuki, T.; McCormick, P. G. Mechanochemical synthesis of nanoparticles. *Journal of Materials Science 2004 39:16* **2004/08**, *39* (16). DOI: 10.1023/B:JMSC.0000039199.56155.f9.
(11) Do, J.-L.; Friščić, T. Mechanochemistry: A Force of Synthesis. *ACS Central Science* **2017**, *3* (1), 13-19. DOI: 10.1021/acscentsci.6b00277 (acccessed 2023-06-08T16:05:22).
(12) Ardila-Fierro, K. J.; Hernández, J. G. Sustainability Assessment of Mechanochemistry by Using the Twelve Principles of Green Chemistry. *ChemSusChem* **2021**, *14* (10), 2145-2162. DOI: 10.1002/cssc.202100478 MEDLINE.

(13) D'Amato, R.; Bondi, R.; Moghdad, I.; Marmottini, F.; McPherson, M. J.; Naïli, H.; Taddei, M.; Costantino, F. "Shake 'n Bake" Route to Functionalized Zr-UiO-66 Metal–Organic Frameworks. *Inorganic Chemistry* **2021**, *60* (18), 14294-14301. DOI: 10.1021/acs.inorgchem.1c01839.
(14) Singh, N. K.; Hardi, M.; Balema, V. P. Mechanochemical synthesis of an yttrium based metal–organic framework. *Chemical Communications* **2013**, *49* (10), 972-974, 10.1039/C2CC36325A. DOI: 10.1039/C2CC36325A.
(15) Užarević, K.; Wang, T. C.; Moon, S.-Y.; Fidelli, A. M.; Hupp, J. T.; Farha, O. K.; Friščić, T. Mechanochemical and solvent-free assembly of zirconium-based metal–organic frameworks. *Chemical Communications* **2016**, *52* (10), 2133-2136. DOI: 10.1039/c5cc08972g (acccessed 2024-06-03T19:42:59).
(16) Rak, M. J.; Saadé, N. K.; Friščić, T.; Moores, A. Mechanosynthesis of ultra-small monodisperse amine-stabilized gold nanoparticles with controllable size. *Green Chem.* **2014**, *16* (1), 86-89. DOI: 10.1039/c3gc41827h.
(17) Chen, Y.; Soler, L.; Xie, C.; Vendrell, X.; Serafin, J.; Crespo, D.; Llorca, J. A straightforward method to prepare supported Au clusters by mechanochemistry and its application in photocatalysis. *Applied Materials Today* **2020**, *21*, 100873. DOI: 10.1016/j.apmt.2020.100873 (acccessed 2024-06-18T20:33:38).
(18) Mechanochemical solid state synthesis of (Cd0.8Zn0.2)S quantum dots: Microstructure and optical characterizations. *Journal of Alloys and Compounds* **2011/03/10**, *509* (10). DOI: 10.1016/j.jallcom.2011.01.035.
(19) Synthesis and characterization of Zn1-xAcxS (0≤x≤0.1) nanocrystalline quantum dots prepared via soft mechanochemical approach. *Ceramics International* **2019/11/01**, *45* (16). DOI: 10.1016/j.ceramint.2019.07.082.
(20) Friščić, T. New opportunities for materials synthesis using mechanochemistry. *Journal of Materials Chemistry* **2010**, *20* (36). DOI: 10.1039/c0jm00872a.
(21) Jin, T.; Liu, T.; Hajiali, F.; Santos, M.; Liu, Y.; Kurdyla, D.; Régnier, S.; Hrapovic, S.; Lam, E.; Moores, A. High-Humidity Shaker Aging to Access Chitin and Cellulose Nanocrystals**. *Angewandte Chemie* **2022**, *134* (42). DOI: 10.1002/ange.202207206 (acccessed 2024-08-08T16:00:39).
(22) Chaudhuri, H.; Karak, N. Water dispersed bio-derived transparent polyurethane: Synthesis, properties including chemical resistance, UV-aging, and biodegradability. *Progress in Organic Coatings* **2020**, *146*, 105730. DOI: https://doi.org/10.1016/j.porgcoat.2020.105730.
(23) Cliffe, M. J.; Mottillo, C.; Stein, R. S.; Bučar, D.-K.; Friščić, T. Accelerated aging: a low energy, solvent-free alternative to solvothermal and mechanochemical synthesis of metal–organic materials. *Chemical Science* **2012**, *3* (8), 2495-2500. DOI: 10.1039/c2sc20344h (acccessed 2023-05-16T14:51:53).
(24) Debnath, D.; Kim, S. H.; Geckeler, K. E. The first solid-phase route to fabricate and size-tune gold nanoparticles at room temperature. *Journal of Materials Chemistry* **2009**, *19* (46). DOI: 10.1039/b905260g.
(25) Richard, A. J.; Ferguson, M.; Fiss, B. G.; Titi, H. M.; Valdez, J.; Provatas, N.; Friščić, T.; Moores, A. In situ study of Au nanoparticle formation in a mechanochemical-aging-based method. *Nanoscale Advances* **2023**, *5* (10), 2776-2784. DOI: 10.1039/d2na00759b (acccessed 2023-05-31T16:15:33).
(26) Ferguson, M.; Richard, A. J.; Valdez, J.; Fiss, B. G.; Titi, H. M.; Provatas, N.; Friscic, T.; Moores, A. Direct observation by high resolution transmission electron microscopy of gold(III) particle transformation during aging reduction reaction. *Faraday Discuss* **2022**. DOI: 10.1039/d2fd00126h From NLM Publisher.
(27) Koper, M. T. M. Structure sensitivity and nanoscale effects in electrocatalysis. *Nanoscale* **2011**, *3* (5), 2054-2073, 10.1039/C0NR00857E. DOI: 10.1039/C0NR00857E.

(28) Stefanovic, P.; Haataja, M.; Provatas, N. Phase field crystal study of deformation and plasticity in nanocrystalline materials. *Physical Review E* **2009-10-13**, *80* (4). DOI: 10.1103/PhysRevE.80.046107.
(29) Chen, C.-C.; Zhu, C.; White, E. R.; Chiu, C.-Y.; Scott, M. C.; Regan, B. C.; Marks, L. D.; Huang, Y.; Miao, J. Three-dimensional imaging of dislocations in a nanoparticle at atomic resolution. *Nature* **2013**, *496* (7443), 74-77. DOI: 10.1038/nature12009 (acccessed 2024-09-20T14:23:20).
(30) Sinno, T.; Dornberger, E.; von Ammon, W.; Brown, R. A.; Dupret, F. Defect engineering of Czochralski single-crystal silicon. *Materials Science and Engineering: R: Reports* **2000**, *28* (5), 149-198. DOI: https://doi.org/10.1016/S0927-796X(00)00015-2.
(31) Rabeya, R.; Mahalingam, S.; Manap, A.; Satgunam, M.; Akhtaruzzaman, M.; Chia, C. H. Structural defects in graphene quantum dots: A review. *International Journal of Quantum Chemistry* **2022**, *122* (12). DOI: 10.1002/qua.26900 (acccessed 2024-06-18T17:23:34).
(32) Tang, Y.; Ouyang, M. Tailoring properties and functionalities of metal nanoparticles through crystallinity engineering. *Nature Materials* **2007**, *6* (10), 754-759. DOI: 10.1038/nmat1982 (acccessed 2024-02-26T19:09:06).
(33) Lu, L.; Shen, Y.; Chen, X.; Qian, L.; Lu, K. Ultrahigh Strength and High Electrical Conductivity in Copper. *Science* **2004**, *304* (5669), 422-426. DOI: 10.1126/science.1092905 (acccessed 2024-02-26T19:52:11).
(34) Do, J.-L.; Mottillo, C.; Tan, D.; Štrukil, V.; Friščić, T. Mechanochemical Ruthenium-Catalyzed Olefin Metathesis. *Journal of the American Chemical Society* **February 12, 2015**, *137* (7). DOI: 10.1021/jacs.5b00151.
(35) Adam, P.-M.; Benrezzak, S.; Bijeon, J. L.; Royer, P. Localized surface plasmons on nanometric gold particles observed with an apertureless scanning near-field optical microscope. *Journal of Applied Physics* **2000**, *88* (11), 6919-6921. DOI: 10.1063/1.1323528 (acccessed 7/15/2024).
(36) Davey, W. P. Precision Measurements of the Lattice Constants of Twelve Common Metals. *Physical Review* **1925**, *25* (6), 753-761. DOI: 10.1103/PhysRev.25.753.
(37) Tsirelson, V.; Stash, A. Orbital-free quantum crystallography: view on forces in crystals. *Acta Crystallographica Section B Structural Science, Crystal Engineering and Materials* **2020**, *76* (5), 769-778. DOI: 10.1107/s2052520620009178 (acccessed 2024-06-27T18:11:10).
(38) Schneider, C. A.; Rasband, W. S.; Eliceiri, K. W.; Schneider, C. A.; Rasband, W. S.; Eliceiri, K. W. NIH Image to ImageJ: 25 years of image analysis. *Nature Methods 2012 9:7* **2012-06-28**, *9* (7). DOI: 10.1038/nmeth.2089.
(39) Wojdyr, M.; Wojdyr, M. Fityk: a general-purpose peak fitting program. *urn:issn:0021-8898* **2010-09-10**, *43* (5). DOI: 10.1107/S0021889810030499.
(40) Atkins, P. W.; De Paula, M. J. *Chimie physique*; De Boeck Supérieur, 2013.

2.8 Supplementary Information

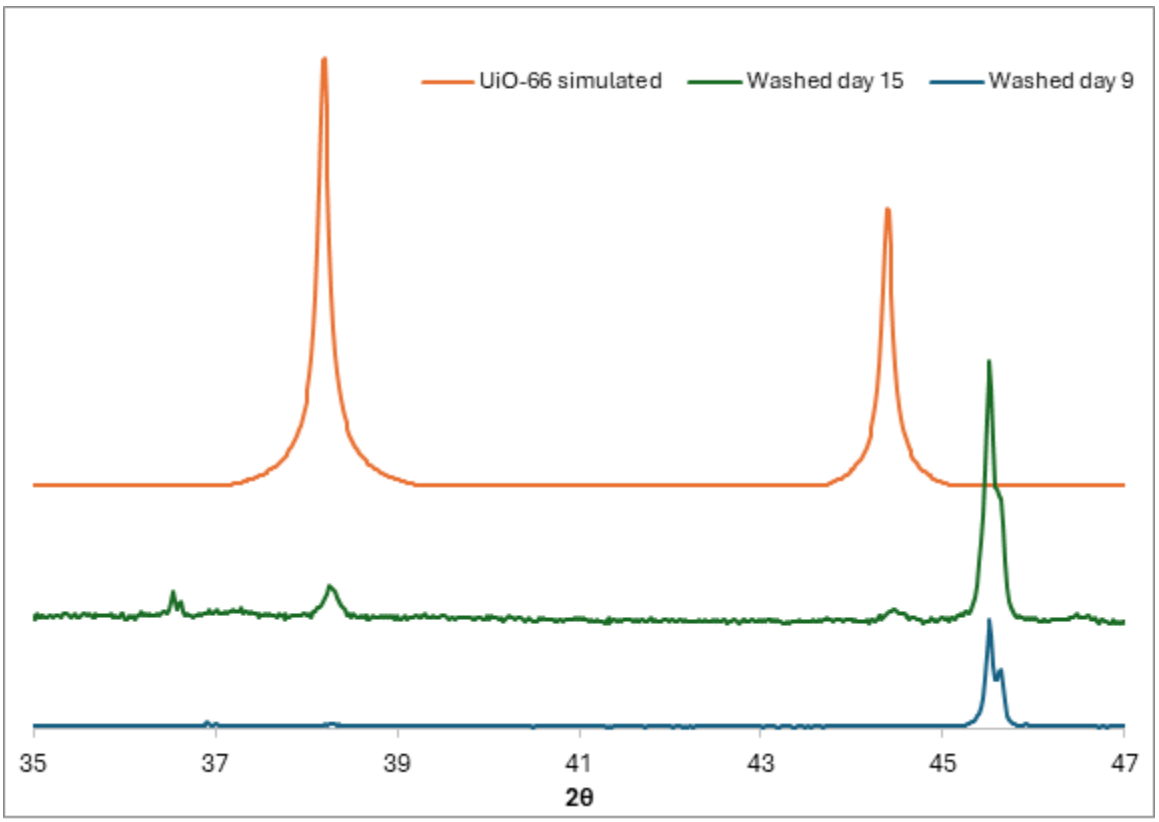

Figure 2.6 XRD spectrum of washed ODA capped AuNPs sample after 9 and 15 days aging.

Table 2.1 Numerical values of AuNPs measured for each samples.

Sample	Crystallinity	Number of NPs			
		Size (nm)			
		0-2	3 to 4	5 to 6	7 to 8
ODA RT	single crystal	494	14	9	4
	single twin	0	0	0	1
	multi-twin	0	0	0	0
	polycrystalline	56	10	17	4
	other defects	0	2	3	1
DODE RT	single	660	38	3	4
	single twin	0	4	2	0
	multi-twin	0	0	2	1
	polycrystalline	118	30	5	7
	other defects	0	5	1	0
ODA 15°	single	318	32	3	5
	single twin	1	1	0	0
	multi-twin	0	0	0	2
	polycrystalline	11	11	9	5
	other defects	0	1	0	1
DODE 15°	single	697	34	4	2
	single twin	1	1	0	0
	multi-twin	0	0	0	0
	polycrystalline	67	28	6	7
	other defects	1	4	1	2

3 Study of UiO-66 formation grown via solid-state aging techniques

The primary emphasis of this chapter is on the synthesis of UiO-66. After gaining a more comprehensive understanding of how AuNPs crystallize in the solid-state, we explored the crystallization process of a metal-organic framework also grown in a solid-state manner. Starting from previous work that developed a UiO-66 synthesis method based on aging and mechanochemistry, we investigated different methods of synthesis which would allow for an ambient condition aging system. Though our initial intention was to observe the crystallization using high-resolution transmission electron microscopy and connected techniques such as electron energy loss spectroscopy, our inability to successfully replicate the findings published in the literature prevented fulfillment of our objectives. It is crucial to have a good understanding of metal-organic frameworks crystallization in order to better plan synthesis. In this chapter, we will provide a description of the parameters that we explored and present an analysis of the milled powder obtained through the combination of a zirconium metal salt or an acetate cluster with an organic linker and modulator.

This chapter is based on a manuscript in preparation and is presented with permission from all co-authors.

3.1 Abstract

Metal-organic frameworks (MOFs) are highly porous materials composed of metal clusters and organic linkers, with UiO-66, a zirconia-based MOF, known for its exceptional stability and wide range of applications, such as gas adsorption and catalysis. Traditional synthesis methods, such as solvothermal processes, are resource-intensive and often involve toxic solvents, making them less environmentally friendly. Green synthesis techniques, including mechanochemistry, liquid-assisted grinding and aging, were used in attempts to develop a solventless aging method of UiO-66 synthesis. Despite various attempts, fully crystalline UiO-66 was not successfully formed, as established by Powder X-ray diffraction and High-resolution transmission electron microscopy results. Once we can establish a synthetic path for this material our goal is to study its crystallization in the solid phase.

3.2 Introduction

Metal-organic frameworks (MOFs) are porous and tunable materials composed of organic linkers and metal clusters, also called secondary-building unit (SBU).[1] UiO-66 is an incredibly stable zirconia based MOF of *fcu*-topology first reported by Cavka et al.[2] Its synthesis involved a solvothermal reaction, where a zirconium salt and organic ligand, terephthalic acid, were combined and heated in dimethylformaldehyde (DMF) overnight.[2] UiO-66 has a variety of applications such as gas adsorption because of its high stability, even during the adsorption and desorption process.[3, 4] UiO-66 was also proven to have some functionality in the biology industry as a biomimetic catalyst for the hydrolysis of methyl paraoxon.[5] Since UiO-66 has such useful properties, the use of this material in industry settings is becoming increasingly popular.[6] Because of this, large-scale synthesis of MOFs has also been a great point of interest. Unfortunately, since the synthesis usually

involves a one-pot solvothermal, microwave or electrochemical method[7], the amount of needed solvents, sometimes toxic, has potential incremental consequences.

Mechanochemistry, on the other hand, has been suggested as a solution to this longstanding issue. For instance, the green synthesis of $Cu_3(BTC)_2$ using twin screw extrusion was developed, which allowed for high yield in a continuous manufacturing setting.[8] This synthesis required minimal amount of solvent, with water being the only by-product of said synthesis, and could be applied to a variety of other MOFs.[8] Adding catalytic amounts of solvents such as water, a mechanochemistry method called liquid-assisted grinding (LAG), is often used in the green synthesis of MOFs.[9, 10] This addition to a mechanochemical reaction is frequently used because it can accelerate or even enable the reaction.[9] Another method of synthesis, which usually forms highly crystalline MOFs, involves the formation of the metal cluster as a precursor to MOF synthesis.[11] Using this method allows for a better control of the crystallization and formation UiO-66 derivatives simply by selecting different linkers.[12]

Aging is a technique used by researchers to form MOFs. The solventless method is a green alternative to other methods and can involve multiple parameters, such as temperature[13], humidity and pressure.[14] D'Amato et al. developed a synthesis using aging at elevated temperatures to form UiO-66.[15] Mixing together a zirconium metal salt, a linker and a catalytic amount of liquid, they were able to achieve highly crystalline UiO-66. Depending on the pKa of the chosen linker, the ratio of acetic acid to water changed to improve crystallinity, the liquid acting as a modulator in the reaction.[15] It would be beneficial to understand how the reaction conditions affect the crystallinity and pore size of the material, considering the properties are dependent on the presence or absence of defects.[16] UiO-66, being considered one of the most stable MOF because of its cluster being 12-connected, compared to the common 4 to 6, can sustain more defects without

collapsing.[16] Shearer et al. found that increasing the temperature and ratio of linker promoted the binding of the linker to the metal, forming a MOF with fewer defects.[17] MOFs containing defects, being either a missing metal cluster or a missing linker, are usually characterized by powder Xray diffraction (PXRD), thermogravimetric analysis (TGA), Brunauer–Emmett–Teller (BET), nuclear magnetic resonance (NMR) or Fourier transform infra red (FTIR).[16] These methods are good to prove the existence of defects and give additional information, such as pore size of the structure but none are able to quantify them. Transmission-electron microscopy (TEM) might be a good solution to this problem. Unfortunately, MOFs are notoriously hard to image via TEM because of their tendency to collapse when they are under the TEM electron beam.[18] Wiktor et al. were able to image MOF-5 using high-resolution TEM (HR-TEM). The group used aberration correction, liquid nitrogen atmosphere and low acceleration voltage to image defect free MOF-5.[18] Liu et al. were able to image solvothermally synthesized defective UiO-66 using HR-TEM.[19] Using formic acid to promote defects resulted in a UiO-66 containing a great amount of defects, as showed by powdered x-ray diffraction (PXRD), with cluster defects become rarer as crystallization time extends.[19] A missing linker defect can be observed by PXRD while a missing cluster has a PXRD spectrum equivalent to the one without defects. This demonstrates that one of the only ways to observe cluster defects is to use HR-TEM.[19]

In this paper we observed the solid-state formation of UiO-66-NO_2 via HR-TEM. We used a complimentary method, Electron Energy-Loss spectroscopy (EELS) as a means to observe the mobility of each element during a 48hrs aging period. Scanning transmission electron microscopy (STEM) and Electron energy loss (EELS) were used to map the formation of the MOF for a 48hrs period.

3.3 Discussion

The synthesis, mechanochemical or not, of UiO-66 is often accompanied by the presence of a modulator. The modulator has an important role because of the competition it generates with the linker by containing only one coordination type, which forms more crystalline MOFs.[3] Following the literature detailing a one-pot aging synthesis of UiO-66, we started by milling Zr metal salt ($ZrOCl_2 \cdot 8H_2O$), organic linker (NO_2-BDC) and a modulator (acetic acid) together (Fig.3.1).[15]

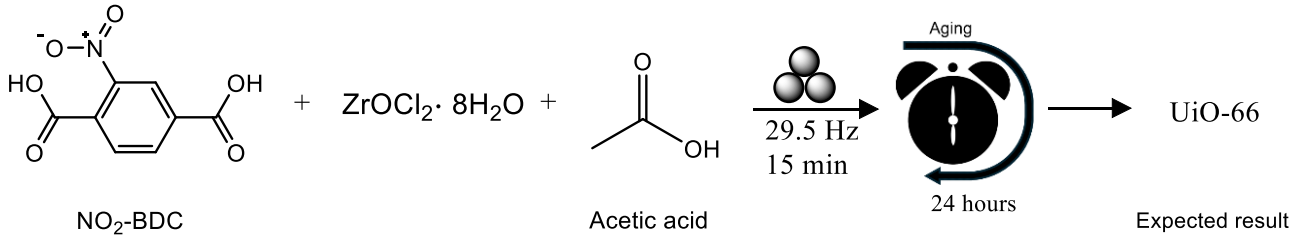

Figure 3.1 Reported synthesis of UiO-66 by mechanochemical mixing for 15 min, followed by aging 21 °C for 24 hours.

Adding acetic acid resulted in a slurry which dried while aging and was brought to PXRD for analysis (Fig. 3.1). To avoid the influence of solvents on the MOF crystallization, we avoided any washing of our sample after synthesis.

With UiO-66 showing prominent peaks at $2\theta = 7.36°$ and $8.52°$ in PXRD spectrums, we used these peaks to analyze the structure of the MOF.

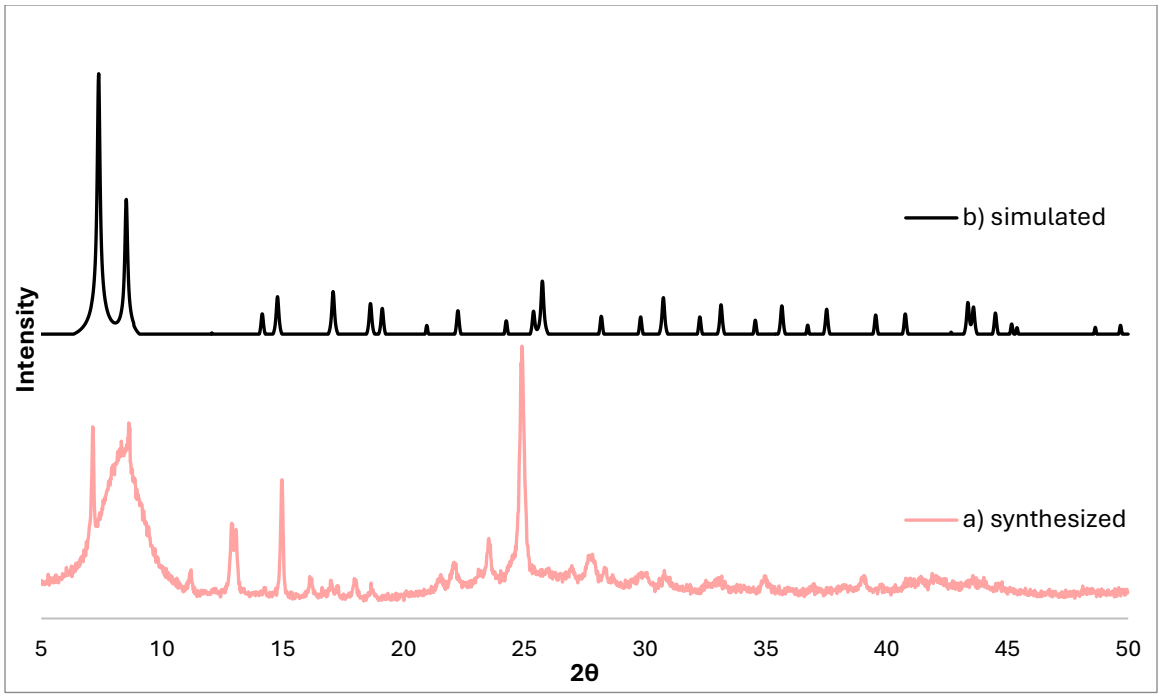

Figure 3.2 XRD spectrum of ZrOCl2 • 8H2O, acetic acid and NO2-BDC milled together for 15 minutes a) after aging 24hrs and b) UiO-66 simulated

Figure 3.2 shows that PXRD peaks are shifted from the expected peaks, with 2θ = 7.14° and 8.66°. The peaks were also broader, showing poor crystallinity. We also observe the absence of a few other UiO-66 peaks such as the peak at 2θ = 25.76°, indicating that the MOF was not formed during milling or aging.

Following D'Amato et al., we decided to introduce an acidic modulator, and picked uric acid as a solid one, as opposed to liquid ones used before (Fig. 3.3).

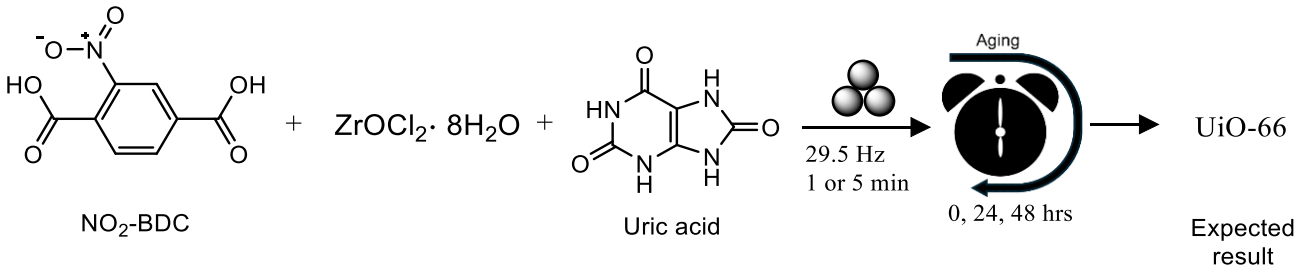

Figure 3.3 Attempted synthesis of UiO-66 by mechanochemical mixing with uric acid for 1 or 5 min, followed by aging 21 °C for up to 48 hours.

As observed in Figure 3.4, aging the sample for 24hrs results in a peak shift. While right after milling $ZrOCl_2 \cdot 8H_2O$, NO_2-BDC and uric acid together showed peaks at 2θ = 7.67° and 8.63°, after 24hrs, a third peak starts to form at 2θ = 7.09°, with the peak at 2θ = 7.67° becoming less prevalent, indicating a reaction in the sample during aging. Other peaks in the sample can be attributed to reagents.

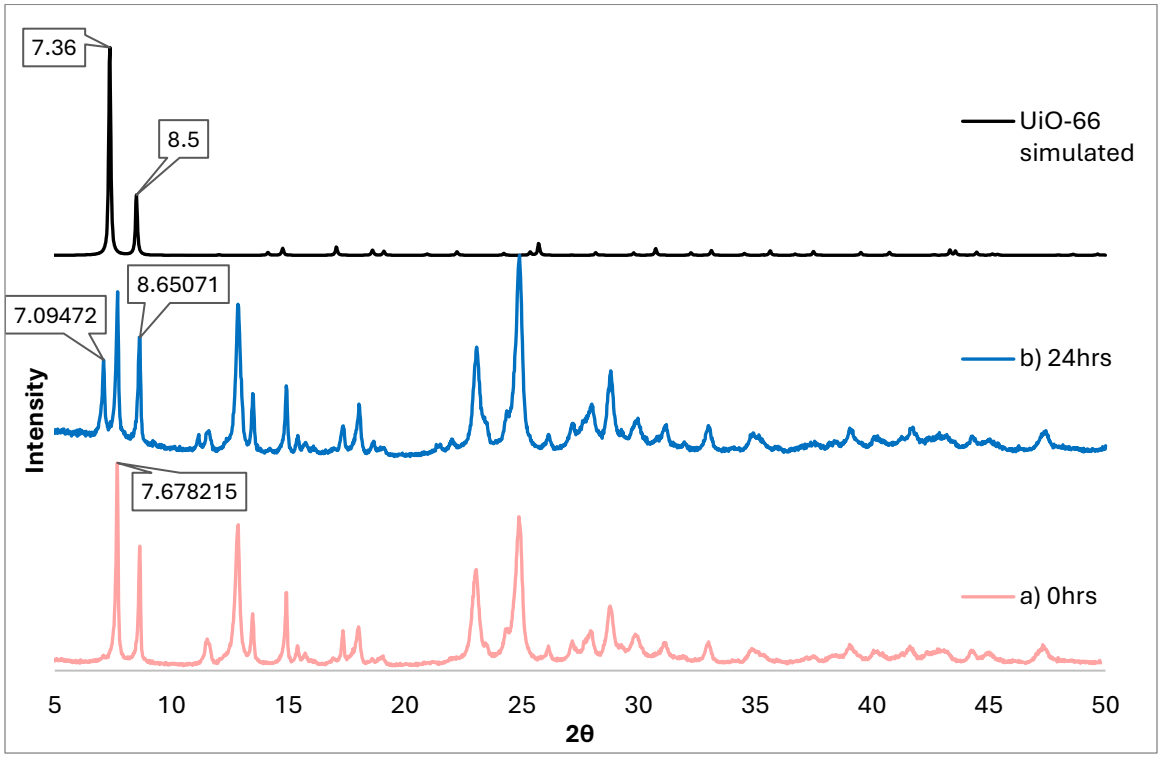

Figure 3.4 PXRD spectrum of milled sample containing Zr metal salt, Uric acid and 2-nitroterephthalic acid aged for a)0hrs and b)24hrs after milling 1 minute.

We understand that while we are not forming UiO-66, we are making a crystalline material. Thinking that the peaks observed were from the presence of the Zr metal cluster, we milled and aged the Zr metal salt with uric acid without the presence of linker (Fig. 3.5).

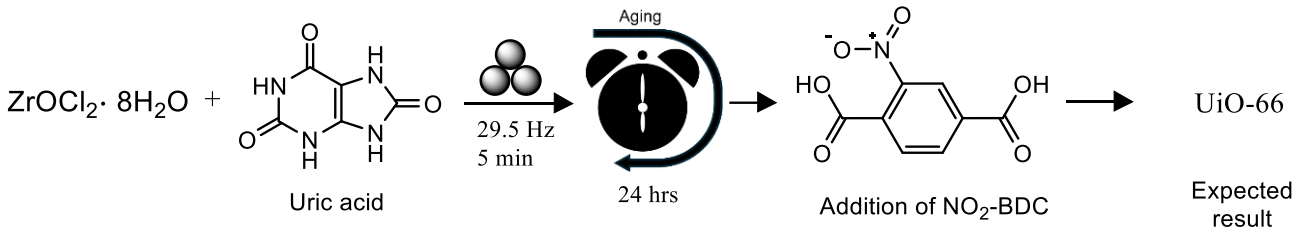

Figure 3.5 Attempted synthesis of UiO-66 by mechanochemical mixing of Zr metal salt and modulator for 5 min, followed by aging 21 °C for 24 hours before the addition of NO2-BDC and milling for 5 min.

During aging, the milled sample containing $ZrOCl_2 \cdot 8H_2O$ and uric acid shows small changes in peaks where peaks became stronger and sharper after aging (Fig. 3.6a,b).

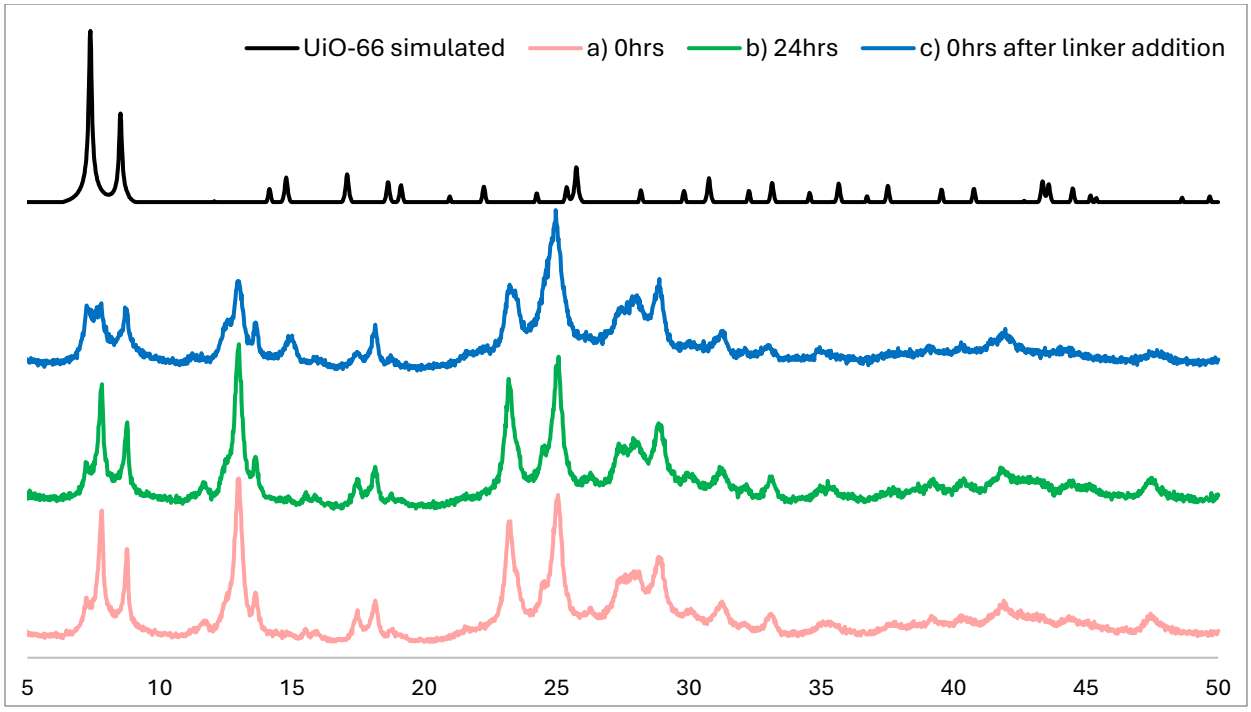

Figure 3.6 PXRD spectrum of milled Zr metal salt and Uric acid after a)0hrs and b)24hrs and c) after addition of 2-nitroterephthalic acid. Both a) and c) were milled for 5 minutes.

We also observed the three previously predominant peaks at 2θ = 7.27°, 8.06° and 8.77° losing intensity after the addition of the linker (Fig. 3.6c). The presence of all three peaks even with the absence of any linker indicates that the peaks observed are not from the metal cluster and are an indication that a different material is synthesised.

After asserting that using a zirconia metal salt precursor was unlikely to result in crystalline MOF, we decided on using a metal cluster as a starting point to form UiO-66 following the example of Karadeniz et al (Fig. 3.7 and 3.8).[10]

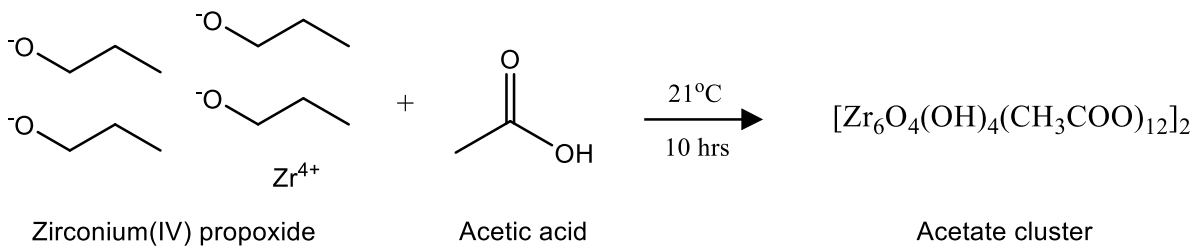

Figure 3.7 Synthesis of Acetate cluster by mixing of Zirconium (IV) propoxide and acetic acid, followed by aging 21 °C for 10 hrs

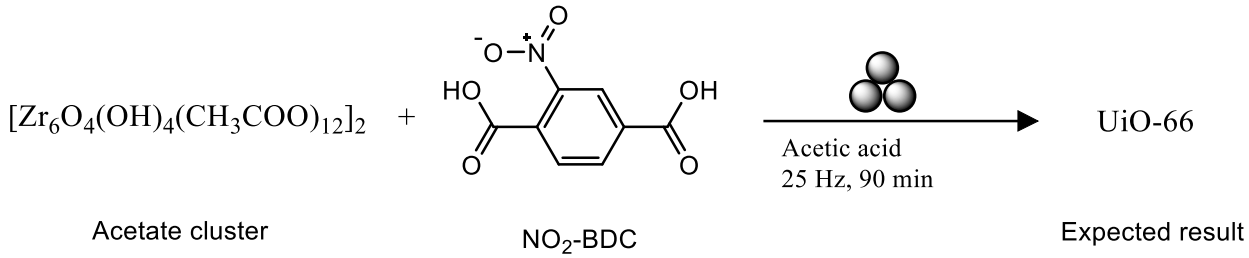

Figure 3.8 Attempted synthesis of UiO-66 by mechanochemical mixing of Acetate cluster, NO2-BDC and acetic acid for 90 min.

The acetate cluster was synthesized by combining acetic acid and zirconium(IV) propoxide (70 wt% 1-propanol solution), as detailed in the experimental section, and analyzed via PXRD to verify the structure and crystallinity (Fig. 3.9).

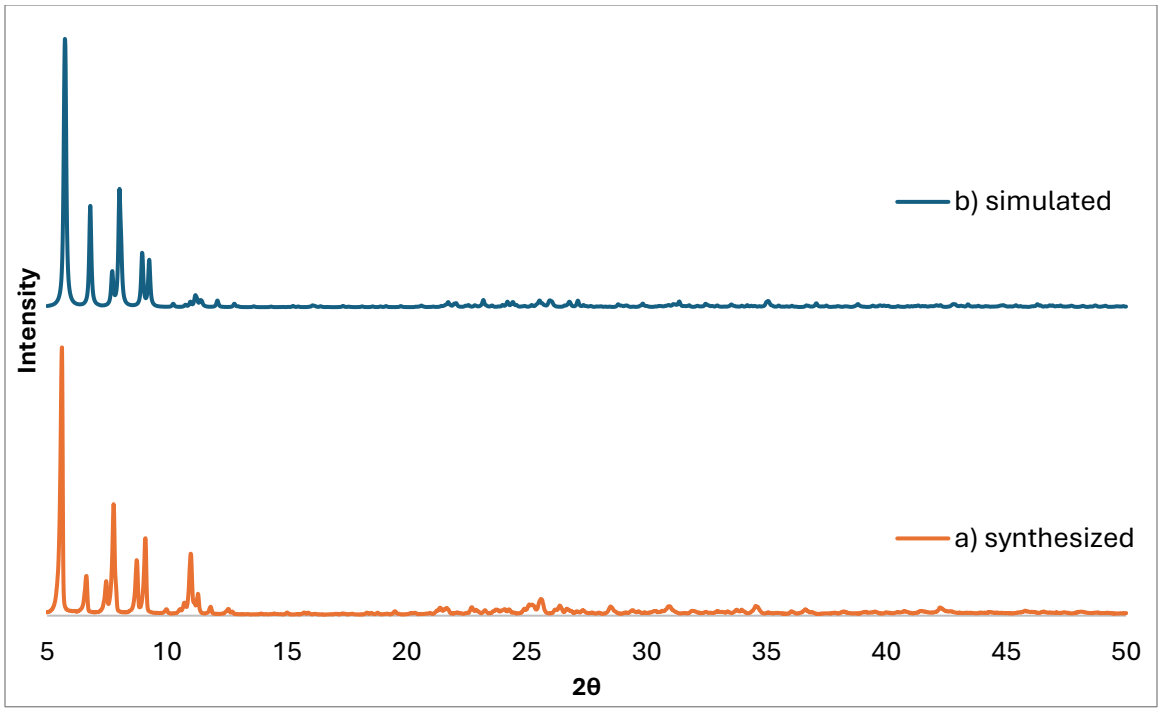

Figure 3.9 PXRD spectrum of Acetate cluster a) synthesized and b) simulated

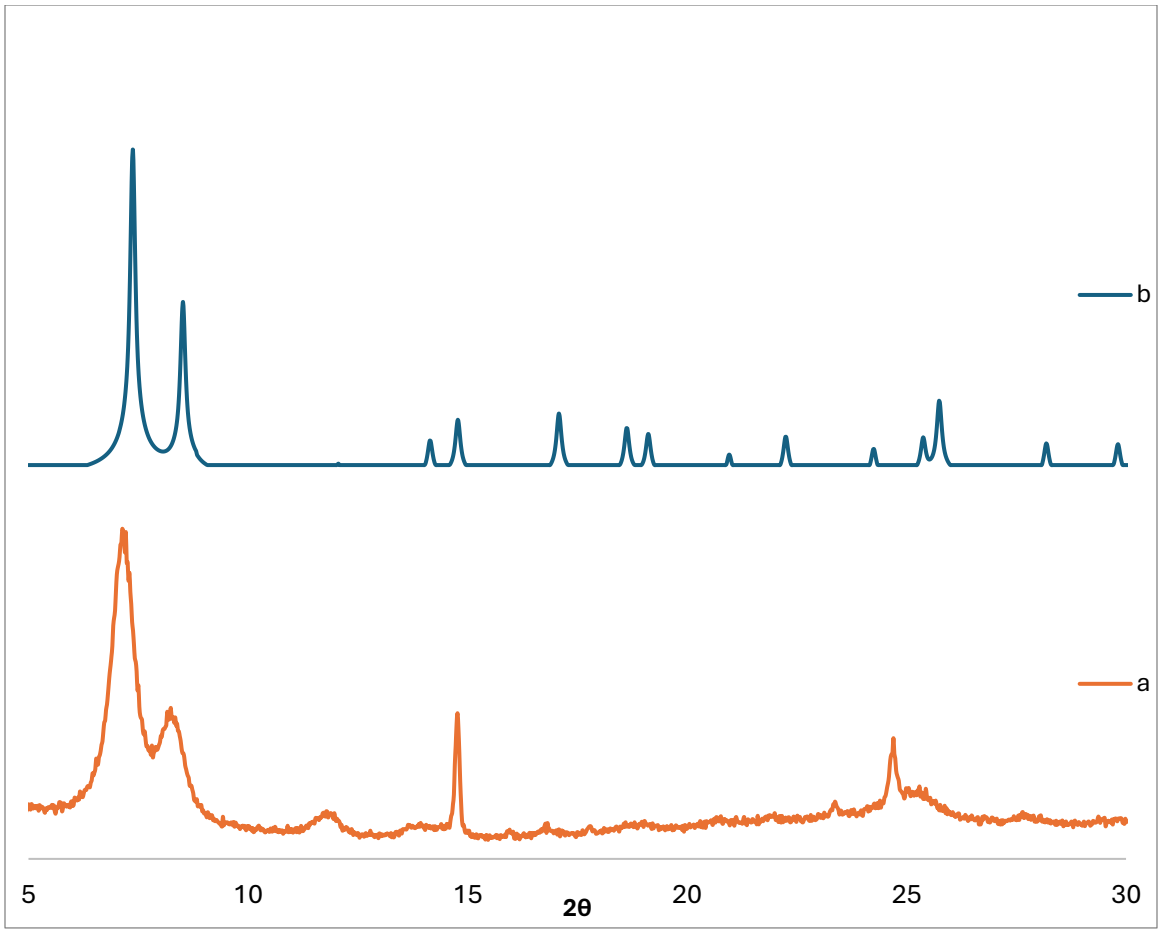

Figure 3.10 PXRD spectrum of ZrOCl2 • 8H2O, acetic acid and NO2-BDC milled together for 90 minutes a) synthesized and b) UiO-66 simulated.

The major peaks in Figure 3.10a indicate that UiO-66 was not successfully formed. Both being shifted from different amounts when compared to the simulated peaks, we are unable to confirm the formation of UiO-66. This could be because of the difference in organic linker compared to the one in the literature, where we used NO^2-BDC or terephthalic acid (BDC) and the literature used 2-aminoterephthalic acid (NH_2-BDC). We believe that the source of the problem might be the difference in pK_a between the two linkers, NH_2-BDC used in the literature and NO_2-BDC used in our experiments, which would be different enough to be changing the material formed during milling. This would have to be explored further. In order to further confirm this, the sample was brought to TEM for imaging. To avoid any solvent influence on the crystallization of the system,

the TEM grids were not prepared using a drop-casting method but by a solid-state process, as detailed in the experimental section.

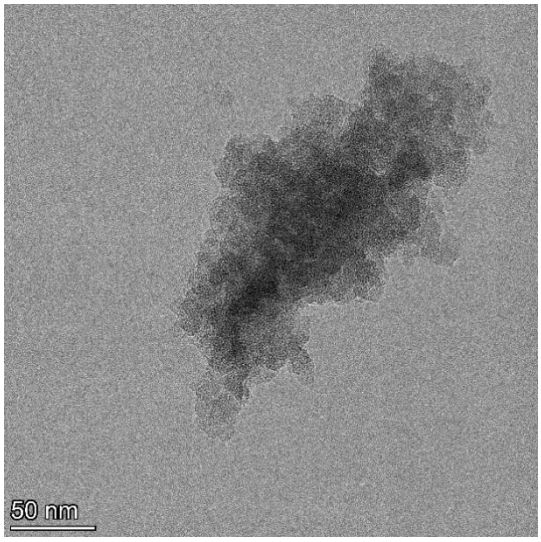

Figure 3.11 TEM images of milled sample containing acetate cluster, acetic acid and NO2- BDC.

Even though no discernable shapes were observed through TEM (Fig. 3.11), EDX showed the presence of all components, such as zirconia and nitrogen, expected in UiO-66. Fast-Fourier Transform (FFT) images of the material display a lack of crystallinity. This could be because of the high amount of instantaneous burning from the HR-TEM electron beam, as expected for a material that is mainly composed of organic material. This sensitivity could also be because of the lack of stability usually provided by the specific structure of UiO-66.

3.4 Conclusion

In conclusion, despite multiple attempts, the mechanochemical synthesis of fully crystalline UiO-66 was not achieved. PXRD spectra showed peak shifts and broadening, indicating the formation of a different crystalline material instead of the desired MOF. Neither the use of uric acid nor a

pre-formed zirconia acetate cluster successfully resulted in the synthesis of UiO-66. HR-TEM confirmed the presence of the expected elemental components but showed no crystallinity, likely due to the material's sensitivity to the electron beam. Once UiO-66 is successfully synthesized, performing an EELS map of the material would be a valuable complementary method to HR-TEM, as it would allow for tracking the distribution of key elements, such as zirconium and nitrogen, during crystallization. Future research should focus on exploring alternative linkers, reaction conditions, and modulators to overcome synthesis challenges and produce a stable, defect-controlled UiO-66 structure.

3.5 Experimental

Acetic acid

$ZrOCl_2 \cdot 8H_2O$ (604.2 mg, 1.875 mmol), acetic acid (0.5 mL, 8.72 mmol) and 2-nitroterephthalic acid (395.8g, 1.875 mmol) were added to a 15ml zirconia milling jar (Form-Tech Scientific) with an 8mm (3.0 g) diameter zirconia milling ball. The jar containing the reactants was milled for 5 minutes at 25 Hz on a Retsch MM400 mixer mill. The sample was aged in a dark space at room temperature.

Uric acid

$ZrOCl_2 \cdot 8H_2O$ (116.8 mg, 0.363 mmol), uric acid (106.6 mg, 0.634 mmol) and 2-nitroterephthalic acid (76.5 mg, 0.363 mmol) were added to a 15ml zirconia milling jar (Form-Tech Scientific) with an 8mm (3.0 g) diameter zirconia milling ball. The jar containing the reactants was milled for 5 minutes at 25 Hz on a Retsch MM400 mixer mill. The sample was aged in a dark space at room temperature.

Acetate cluster, $[Zr_6O_4(OH)_4(CH_3COO)_{12}]_2$, synthesis was done according to literature.[10]

Acetic acid (3.50mL) and Zirconium(IV) propoxide (70 wt% 1-propanol solution)(1g, 3.05mmol) were mixed in a sealed jar and left for 10hrs at room temperature (20:1 ratio). The white powder was collected by filtration and dried at room temperature under vacuum.

UiO-66 through the acetate cluster

The Acetate cluster (64.8 mg, 0.023 mmol) and 2-nitroterephthalic acid (50.77 mg, 0.28 mmol) were added to a 10ml teflon milling jar (Form-Tech Scientific) with two 8mm (3.0 g) diameter stainless steel milling ball. The jar containing the reactants was milled for 90 minutes at 25 Hz on a Retsch MM400 mixer mill.

Characterization

The TEM studies were performed using a Thermo Scientific Talos F200X transmission electron microscope equipped with a high-brightness XFEG Schottky source, operated at 200 keV. Images were captured in the high contrast mode. TEM grids were prepared using the solid-state method, where the 400 mesh Cu grid was dipped in the milled powder and any excess powder was removed with a compressed air can.

PXRD studies were performed using a Bruker D8 Advance diffractometer equipped with a Ni-filtered CuKα (λ = 1.5418 Å) source, 1D LYNXEYE detector, and operating at 40kV and 40 mA. PXRD patterns were obtained in a 2θ range of 3° to 50° with an exposure time of 0.70 s and in increments of 0.02°.

3.6 Acknowledgment

We thank the Natural Science and Engineering Research Council of Canada (NSERC) - Discovery Grant and Discovery Accelerator Supplement, the Canada Foundation for Innovation (CFI), the

Centre for Green Chemistry and Catalysis (CGCC), and McGill University for their financial support. We thank Hatem Titi for their contribution to the discussion in the PXRD section of this paper. We thank the Facility for Electron Microscopy Research (FEMR) of McGill University for help in acquiring electron microscopy data. We thank the MC² facility at McGill University for help in acquiring PXRD data.

3.7 References

(1) Jiao, L.; Seow, J. Y. R.; Skinner, W. S.; Wang, Z. U.; Jiang, H.-L. Metal–organic frameworks: Structures and functional applications. *Materials Today* **2019**, *27*, 43-68. DOI: https://doi.org/10.1016/j.mattod.2018.10.038.
(2) Cavka, J. H.; Jakobsen, S.; Olsbye, U.; Guillou, N.; Lamberti, C.; Bordiga, S.; Lillerud, K. P. A New Zirconium Inorganic Building Brick Forming Metal Organic Frameworks with Exceptional Stability. *Journal of the American Chemical Society* **2008**, *130* (42). DOI: 10.1021/ja8057953.
(3) Winarta, J.; Shan, B.; McIntyre, S. M.; Ye, L.; Wang, C.; Liu, J.; Mu, B. A Decade of UiO-66 Research: A Historic Review of Dynamic Structure, Synthesis Mechanisms, and Characterization Techniques of an Archetypal Metal–Organic Framework. *Crystal Growth & Design* **2019**, *20* (2), 1347-1362. DOI: 10.1021/acs.cgd.9b00955.
(4) Furukawa, H.; Cordova, K. E.; O'Keeffe, M.; Yaghi, O. M. The Chemistry and Applications of Metal-Organic Frameworks. *Science* **2013-08-30**, *341* (6149). DOI: 10.1126/science.1230444.
(5) Katz, M. J.; Mondloch, J. E.; Totten, R. K.; Park, J. K.; Nguyen, S. T.; Farha, O. K.; Hupp, J. T. Simple and Compelling Biomimetic Metal–Organic Framework Catalyst for the Degradation of Nerve Agent Simulants. *Angewandte Chemie International Edition* **2014/01/07**, *53* (2). DOI: 10.1002/anie.201307520.
(6) Bazer-Bachi, D.; Assié, L.; Lecocq, V.; Harbuzaru, B.; Falk, V. Towards industrial use of metal-organic framework: Impact of shaping on the MOF properties. *Powder Technology* **2014**, *255*, 52-59. DOI: https://doi.org/10.1016/j.powtec.2013.09.013.
(7) Głowniak, S.; Szczęśniak, B.; Choma, J.; Jaroniec, M. Mechanochemistry: Toward green synthesis of metal–organic frameworks. *Materials Today* **2021**, *46*, 109-124. DOI: https://doi.org/10.1016/j.mattod.2021.01.008.
(8) Crawford, D. E.; Wright, L. A.; James, S. L.; Abbott, A. P. Efficient continuous synthesis of high purity deep eutectic solvents by twin screw extrusion. *Chemical Communications* **2016**, *52* (22), 4215-4218. DOI: 10.1039/c5cc09685e (acccessed 2024-09-13T19:36:52).
(9) Friscic, T.; Reid, D. G.; Halasz, I.; Stein, R. S.; Dinnebier, R. E.; Duer, M. J. Ion- and liquid-assisted grinding: improved mechanochemical synthesis of metal-organic frameworks reveals salt inclusion and anion templating. *Angew Chem Int Ed Engl* **2010**, *49* (4), 712-715. DOI: 10.1002/anie.200906583 From NLM Medline.
(10) Karadeniz, B.; Howarth, A. J.; Stolar, T.; Islamoglu, T.; Dejanović, I.; Tireli, M.; Wasson, M. C.; Moon, S.-Y.; Farha, O. K.; Friščić, T.; et al. Benign by Design: Green and Scalable Synthesis of Zirconium UiO-Metal–Organic Frameworks by Water-Assisted Mechanochemistry. *ACS Sustainable Chemistry & Engineering* **2018**, *6* (11), 15841-15849. DOI: 10.1021/acssuschemeng.8b04458 (acccessed 2023-05-02T17:50:08).

(11) Guillerm, V.; Gross, S.; Serre, C.; Devic, T.; Bauer, M.; Férey, G. A zirconium methacrylate oxocluster as precursor for the low-temperature synthesis of porous zirconium(<scp>iv</scp>) dicarboxylates. *Chem. Commun.* **2010**, *46* (5), 767-769. DOI: 10.1039/b914919h (acccessed 2024-07-22T21:54:59).
(12) Užarević, K.; Wang, T. C.; Moon, S.-Y.; Fidelli, A. M.; Hupp, J. T.; Farha, O. K.; Friščić, T. Mechanochemical and solvent-free assembly of zirconium-based metal–organic frameworks. *Chemical Communications* **2016**, *52* (10), 2133-2136. DOI: 10.1039/c5cc08972g (acccessed 2024-06-03T19:42:59).
(13) Richard, A. J.; Ferguson, M.; Fiss, B. G.; Titi, H. M.; Valdez, J.; Provatas, N.; Friščić, T.; Moores, A. In situ study of Au nanoparticle formation in a mechanochemical-aging-based method. *Nanoscale Advances* **2023**, *5* (10), 2776-2784. DOI: 10.1039/d2na00759b (acccessed 2023-05-31T16:15:33).
(14) Jin, T.; Liu, T.; Hajiali, F.; Santos, M.; Liu, Y.; Kurdyla, D.; Régnier, S.; Hrapovic, S.; Lam, E.; Moores, A. High-Humidity Shaker Aging to Access Chitin and Cellulose Nanocrystals**. *Angewandte Chemie* **2022**, *134* (42). DOI: 10.1002/ange.202207206 (acccessed 2024-08-08T16:00:39).
(15) D'Amato, R.; Bondi, R.; Moghdad, I.; Marmottini, F.; McPherson, M. J.; Naïli, H.; Taddei, M.; Costantino, F. "Shake 'n Bake" Route to Functionalized Zr-UiO-66 Metal–Organic Frameworks. *Inorganic Chemistry* **2021**, *60* (18), 14294-14301. DOI: 10.1021/acs.inorgchem.1c01839.
(16) Feng, Y.; Chen, Q.; Jiang, M.; Yao, J. Tailoring the Properties of UiO-66 through Defect Engineering: A Review. *Industrial & Engineering Chemistry Research* **August 30, 2019**, *58* (38). DOI: 10.1021/acs.iecr.9b03188.
(17) Shearer, G. C.; Chavan, S.; Ethiraj, J.; Vitillo, J. G.; Svelle, S.; Olsbye, U.; Lamberti, C.; Bordiga, S.; Lillerud, K. P. Tuned to Perfection: Ironing Out the Defects in Metal–Organic Framework UiO-66. **July 7, 2014**. DOI: 10.1021/cm501859.
(18) Wiktor, C.; Turner, S.; Zacher, D.; Fischer, R. A.; Tendeloo, G. V. Imaging of intact MOF-5 nanocrystals by advanced TEM at liquid nitrogen temperature. *Microporous and Mesoporous Materials* **2012**, *162*, 131-135. DOI: https://doi.org/10.1016/j.micromeso.2012.06.014.
(19) Liu, L.; Chen, Z.; Wang, J.; Zhang, D.; Zhu, Y.; Ling, S.; Huang, K.-W.; Belmabkhout, Y.; Adil, K.; Zhang, Y.; et al. Imaging defects and their evolution in a metal–organic framework at sub-unit-cell resolution. *Nature Chemistry* **2019**, *11* (7), 622-628. DOI: 10.1038/s41557-019-0263-4 (acccessed 2024-03-21T17:08:33).

4 Discussion and conclusion

This chapter builds on the discussions from Chapters 2 and 3, raising questions and sharing findings that, while relevant to this thesis, did not fit within the more focused manuscripts. It establishes links between these works and earlier research, integrating perspectives from other scholars in the realm of solid-state grown nanoparticles and MOFs, with a focus on their crystalline properties. The chapter will include final remarks and offer suggestions for future research on the topic.

4.1 Discussion of Findings

We start with a review of the results showed in chapter 2 and compare with findings from the relevant literature. Among the papers relevant to chapter 2, one notable article was the synthesis technique developed by Richard et al. This approach involved the use of octadecylamine, gold metal salt, and trisodium citrate to produce octadecylamine capped AuNPs.[1] The process included aging the mixture after 60 seconds of milling. In our own research, we used some of their techniques, such as freezing before milling and the addition of a reducing agent, to conduct a thorough analysis of AuNPs crystallinity and size after an extended aging period.

As presented in chapter 2, most observed particles were in the 0 to 3 nm size range. Richard et al. reported nanoparticles of greater size than ours which we attribute to the drop-cast methods used for TEM analysis which added solvent to the system, an issue we were able to avoid by changing methods and choosing a solid-state grid preparation method.[1] The AuNPs sized in the solid-state is likely to better represent the true system. Rak et al. also reported greater sizes of

mechanosynthesised AuNPs; however, the reaction conditions of the galvanic-reduction mechanochemical method result in substantially different kinetics.[2] In this synthesis, they milled gold metal salt and long chain amines with steel metal balls for 90 minutes, then sonicating the resulting suspension to obtain a powder containing monodisperse AuNPs. They then analysed the HR-TEM images of the resulting AuNPs, capped with different length chain amines, and measured their size (Table 4.1).

Table 4.1 AuNPs aspects and diameters determined by TEM as a function of the ligand[a]. Used with permission of Royal Society of Chemistry, from Ref 2, permission conveyed through Copyright Clearance Center, Inc.

Ligand	AuNP aspects and diameter (nm)
Pentadecylamine (C15)	Spherical – 4.2 ± 1.2
Hexadecylamine (C16)	Spherical – 1.8 ± 0.3
Heptadecylamine (C17)	Spherical – 1.5 ± 0.2
Octadecylamine (C18)	Spherical – 1.3 ± 0.2
4-Dimethylaminopyridine (DMAP)	Incomplete reduction[b]
4,4′-Bipyridine (4,4′ BIPY)	Incomplete reduction[b]
Imidazole	Large irregular particles
1-Methylimidazole	Large irregular particles
Benzyl disulfide	Irregular aggregates
ω-Mercaptododecanoic acid	Films formed on TEM grid
Citrate	Polydisperse large particles ~500 nm

[b]Spherical small NPs are observed by TEM, but XPS analysis demonstrated that mechanosynthesis only afforded partial reduction.

The difference in size found between the long amine chain pentadecylamine (C15) and octadecylamine (C18) was far greater than the one we found between dodecylamine (C12) and octadecylamine (C18). The size of octadecylamine and pentadecylamine capped AuNPs, at around 1.3 nm and 4.2 nm respectively, the effect of the amine chain length is more pronounced than what

we note in chapter 2. They also reported incomplete reduction of the gold salt when using DMAP and 4,4'-Bipyridine, something we also noticed when 12-aminododecanoic acid (ADA) was used in our synthesis.

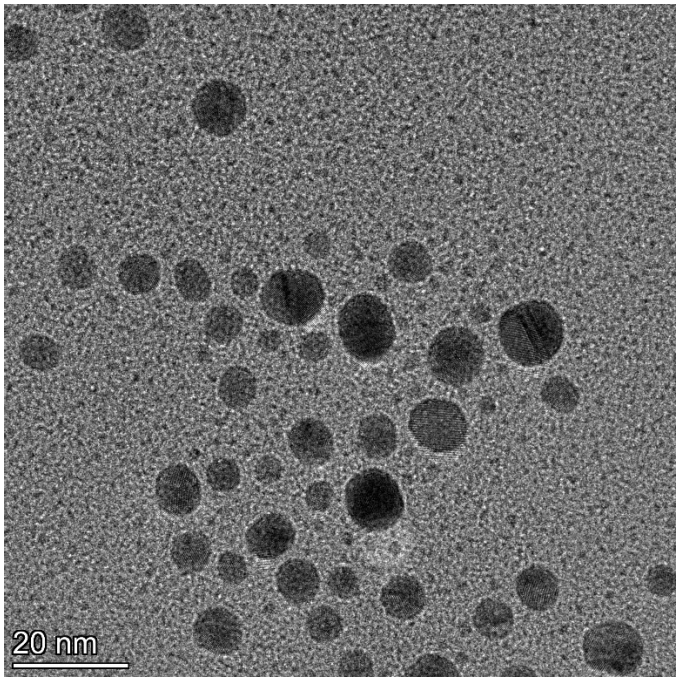

Figure 4.1 HR-TEM image of ADA capped AuNPs after 7 days aging at room temperature.

ADA, containing a carboxyl functional group, was used as a capping agent for the AuNPs synthesis using similar aging conditions as presented in chapter 2 (Fig. 4.1). After aging for 14 days, the sample did not advance to the expected purple colour indicating an incomplete reduction of the gold salt. ADA is a long chain that is terminated on either side by a carboxyl group or amine group. DMAP and 4,4'-Bipyridine, which both resulted in incomplete reductions, both have a melting point of 114 °C; ODA and DODE both have much lower melting points at 52 °C and 30 °C respectively. These high melting points are an indication of the strong intermolecular interactions. Because of the strong dipole-dipole interactions and hydrogen bonding of ADA, the molecular inertia of the solid-state system is much higher than DODE, which slows down the reduction of

gold metal salt. In his 2022 M.Sc. Thesis discussion, A.J. Richard, he mentions the mechanism of AuNPs being a cause for nanoparticle defects such as the ones we studied in chapter 2.[3] He also mentions that the observation of ultrasmall nanoparticles during the aging period suggests that their formation is influenced by sporadic defect formation or amorphization.[3, 4] The ultrasmall particles observed after a short milling time and mild aging conditions demonstrate the small activation barrier required for this mechanism, something the mild aging conditions easily overcame.[3]

Ferguson et al. were interested in exploring the early stages of their own modified Turkevich reaction and used STEM-EELS to image the mobility within the system and the time dependent elemental intensity.[5] Taking inspiration from the results of this paper and results showed in chapter 2, we explored the crystallization of MOFs through EELS, as detailed in chapter 3. We first explored the solid-state synthesis of ZIF-8 because of a previous accelerated aging paper detailing successful synthesis.[6] After milling ZnO, 2-methylimidazole and a salt additive, the powder was aged at 98% relative humidity (RH) at 50-60 °C and analyzed by XRD and TEM.

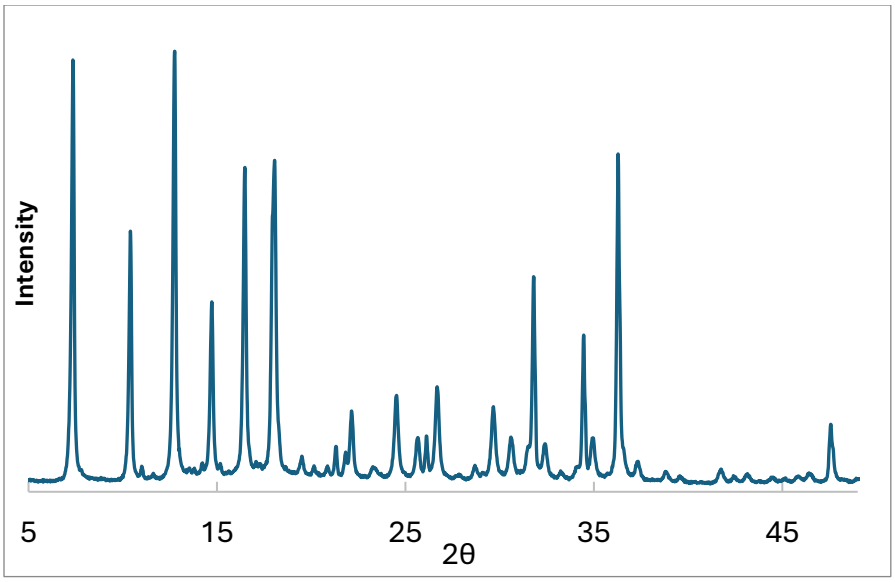

Figure 4.2 PXRD spectrum of unwashed sample, aged at 98% RH at 50-60°C for 24hrs.

Fig.4.2 confirmed the presence of ZIF-8 with peaks at around 2θ = 7.35°, 10.40°, 12.75°, 14.73° and 16.48° being present.[7]

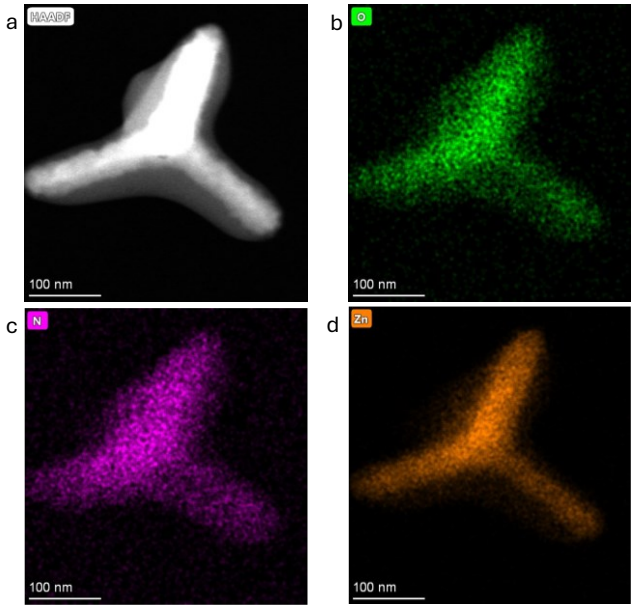

Figure 4.3 STEM-HAADF images (a) and EDX elemental maps for b)O, c)N and d)Zn of unwashed sample aged at 98% RH at 50-60°C for 24hrs.

The TEM images obtained for this sample did not display clear shapes, which would be able to further confirm well crystallized ZIF-8. Figure 4.3 shows EDX spectrum taken of the same sample

showed a proximity between the Zn and C signal, which made it difficult to properly identify points of interest. To counter this, we used Zr-UiO-66 which provides a sharp edge signal in EELS. We followed a synthesis that uses Zr metal salt containing Cl, $ZrOCl_2$,[8] which we could track through an EELS elemental map and assess mobility of these elements and consequently the crystallization of UiO-66.[5] Chapter 3 details the synthesis used where we added acetic acid directly to the milling jar. Besides introducing an additional solvent additive during the milling process, we also subjected the sample to acetic acid vapor aging. Interestingly, the PXRD spectrum remained unchanged when compared to a sample without gas vapor.

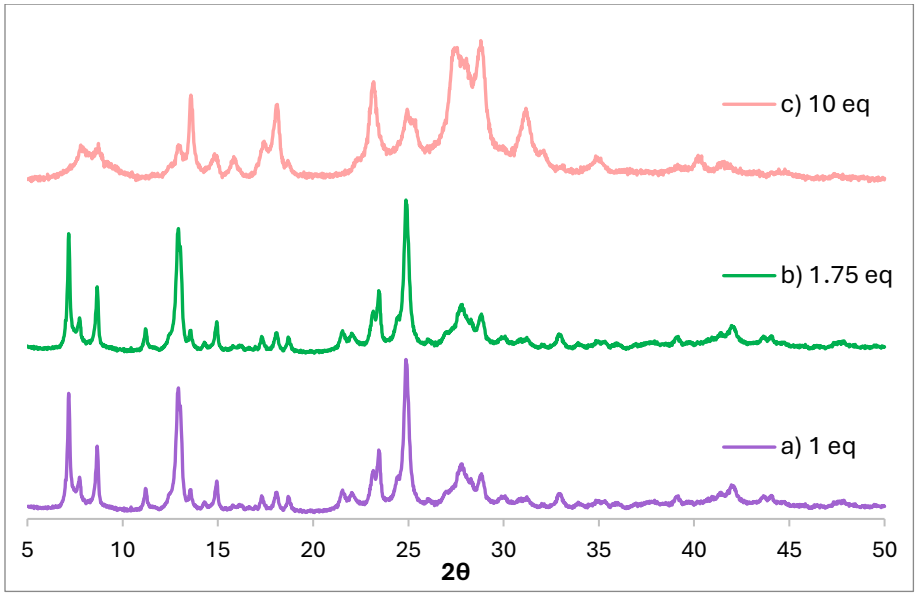

Figure 4.4 PXRD spectrum of unwashed sample containing a)1 eq, b) 1.75 eq and c) 10 eq of uric acid aged for 24hrs.

Considering the addition of uric acid as a modulator, the concentration had to be studied (Fig. 4.4). Too high of a concentration would prevent the MOF from forming while too little results in a MOF of poor crystallinity.[9] As we adjusted the amount of modulator, uric acid, added, the PXRD spectrums showed differences in peaks (Fig. 4.4) whilst showing no formation of UiO-66.

4.2 Conclusion and Future Work

Solid-state formed long chain amine capped AuNPs were imaged and analyzed via HR-TEM. By employing a pre-established solid-state AuNPs synthesis method, a powder comprising gold metal salt, a reducing agent, a solid auxiliary, and a long amine chain was milled briefly. The mixture was then aged at two different temperatures for a duration of 15 days, resulting in a distinct purple colour, a characteristic of AuNPs. Periodically, HR-TEM images of the sample were captured and size and property analysis was conducted on the particles. Using a different length of chain amine, we successfully explored its influence on the size and crystallinity of the formed nanoparticles. When a longer chain amine was used as a capping agent, smaller overall nanoparticles are observed. The colder temperature analyzed showed particles of smaller size, corroborating previous studies asserting the metal reduction dependence on temperature. Combining HR-TEM with a solid-state grid preparation technique prevented the influence of solvent on the reduction and allowed for a more accurate analysis of crystallinity within the system. FFT imaging helped the classification of ultrasmall particles, which showed that shorter chain amines had the tendency to showcase particles with more grain boundaries. This discovery is helpful in pursuing greater crystallinity control for solid-state grown nanoparticles.

Using specialized equipment to understand crystallinity and mobility generated an interest in the crystallization of MOFs grown with solid-state synthesis. After forming ZIF-8 through aging, the sample, when brought to HR-TEM, showed no shape and an extensive sensitivity to the electron beam: the need for a more stable MOF directed us towards UiO-66. Using a Zr metal salt with uric acid and then an acetate cluster with acetic acid, analysis by PXRD and HR-TEM imaging unfortunately did not evidence the formation of the expected UiO-66. With problems such as

selection and ratio of modulator and high sensitivity to the electron beam, successful imaging of the material with HR-TEM still requires a substantial amount of research and technique development.

4.3 References

(1) Richard, A. J.; Ferguson, M.; Fiss, B. G.; Titi, H. M.; Valdez, J.; Provatas, N.; Friščić, T.; Moores, A. In situ study of Au nanoparticle formation in a mechanochemical-aging-based method. *Nanoscale Advances* **2023**, *5* (10), 2776-2784. DOI: 10.1039/d2na00759b (acccessed 2023-05-31T16:15:33).
(2) Rak, M. J.; Saadé, N. K.; Friščić, T.; Moores, A. Mechanosynthesis of ultra-small monodisperse amine-stabilized gold nanoparticles with controllable size. *Green Chem.* **2014**, *16* (1), 86-89. DOI: 10.1039/c3gc41827h.
(3) Richard, A. J. A study of the reduction and formation of gold nanoparticles in the solid state using mechanochemical aging. McGill, 2022.
(4) Malca, M. Y.; Bao, H.; Bastaille, T.; Saadé, N. K.; Kinsella, J. M.; Friščić, T.; Moores, A. Mechanically Activated Solvent-Free Assembly of Ultrasmall Bi2S3 Nanoparticles: A Novel, Simple, and Sustainable Means To Access Chalcogenide Nanoparticles. *Chemistry of Materials* **September 14, 2017**, *29* (18). DOI: 10.1021/acs.chemmater.7b02134.
(5) Ferguson, M.; Richard, A. J.; Valdez, J.; Fiss, B. G.; Titi, H. M.; Provatas, N.; Friscic, T.; Moores, A. Direct observation by high resolution transmission electron microscopy of gold(III) particle transformation during aging reduction reaction. *Faraday Discuss* **2022**. DOI: 10.1039/d2fd00126h From NLM Publisher.
(6) Cliffe, M. J.; Mottillo, C.; Stein, R. S.; Bučar, D.-K.; Friščić, T. Accelerated aging: a low energy, solvent-free alternative to solvothermal and mechanochemical synthesis of metal–organic materials. *Chemical Science* **2012**, *3* (8), 2495-2500, 10.1039/C2SC20344H. DOI: 10.1039/C2SC20344H.
(7) Park, K. S.; Ni, Z.; Côté, A. P.; Choi, J. Y.; Huang, R.; Uribe-Romo, F. J.; Chae, H. K.; O'Keeffe, M.; Yaghi, O. M. Exceptional chemical and thermal stability of zeolitic imidazolate frameworks. *Proceedings of the National Academy of Sciences* **2006**, *103* (27), 10186-10191. DOI: 10.1073/pnas.0602439103 (acccessed 2024-10-08T14:01:50).
(8) D'Amato, R.; Bondi, R.; Moghdad, I.; Marmottini, F.; McPherson, M. J.; Naïli, H.; Taddei, M.; Costantino, F. "Shake 'n Bake" Route to Functionalized Zr-UiO-66 Metal–Organic Frameworks. *Inorganic Chemistry* **2021**, *60* (18), 14294-14301. DOI: 10.1021/acs.inorgchem.1c01839.
(9) Winarta, J.; Shan, B.; McIntyre, S. M.; Ye, L.; Wang, C.; Liu, J.; Mu, B. A Decade of UiO-66 Research: A Historic Review of Dynamic Structure, Synthesis Mechanisms, and Characterization Techniques of an Archetypal Metal–Organic Framework. *Crystal Growth & Design* **2019**, *20* (2), 1347-1362. DOI: 10.1021/acs.cgd.9b00955.